Cell Reports

Article

Dual roles for CND1 in maintenance of nuclear and chloroplast genome stability in plants

Graphical abstract

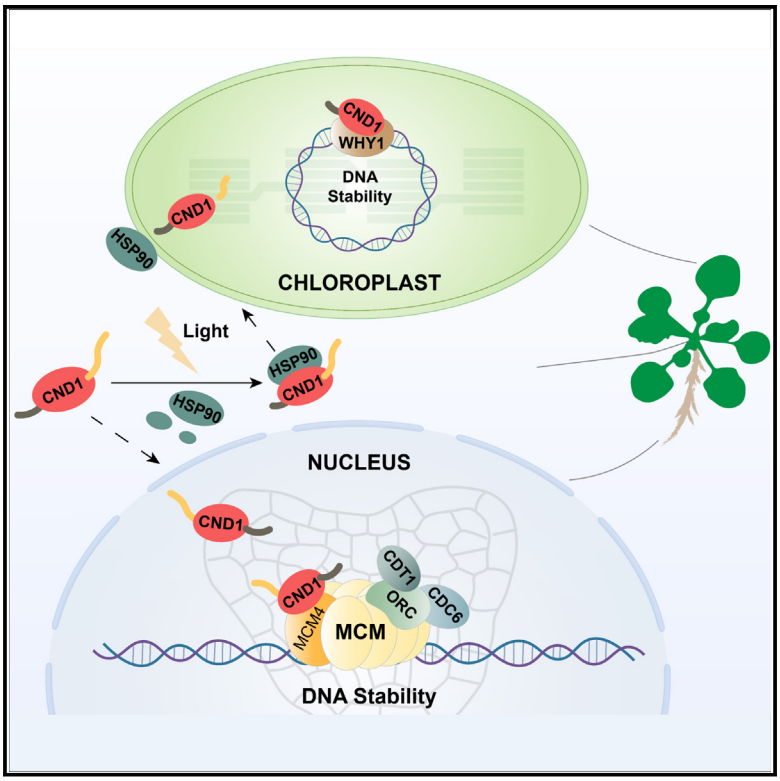

Authors

Hong-Lei Jin, Sujuan Duan, Pengxiang Zhang, ..., Zhenyi Chang, Jiliang Hu, Hong-Bin Wang

Correspondence

jinhl@gzucm.edu.cn (H.-L.J.), wanghongbin@gzucm.edu.cn (H.-B.W.)

In brief

Jin et al. identify a nuclear and chloroplast dual-localized protein CND1 encoded by nuclear gene in higher land plants. CND1 coordinates the status of nuclear and chloroplast genome stability, which is required for plant development and photosynthetic function.

Highlights

- CND1 mutations result in embryo lethality and abnormal development
- CND1 is localized to both nucleus and chloroplast
- CND1 regulates initiation of DNA replication in the nucleus and cell-cycle progression
- CND1 is required for chloroplast genome stability and photosynthetic activity

Jin et al., 2023, Cell Reports *42*, 112268
March 28, 2023
https://doi.org/10.1016/j.celrep.2023.112268

CellPress

Cell Reports

CellPress
OPEN ACCESS

Article

Dual roles for CND1 in maintenance of nuclear and chloroplast genome stability in plants

Hong-Lei Jin,[1,3,6,7,*] Sujuan Duan,[1,6] Pengxiang Zhang,[1] Ziyue Yang,[1] Yunping Zeng,[1] Ziqi Chen,[1] Liu Hong,[1] Mengshu Li,[2] Lujun Luo,[2] Zhenyi Chang,[1] Jiliang Hu,[1] and Hong-Bin Wang[1,4,5,*]

[1]Institute of Medical Plant Physiology and Ecology, School of Pharmaceutical Sciences, Guangzhou University of Chinese Medicine, Guangzhou 510006, People's Republic of China
[2]School of Life Sciences, Sun Yat-sen University, Guangzhou 510275, People's Republic of China
[3]Guangzhou Key Laboratory of Chinese Medicine Research on Prevention and Treatment of Osteoporosis, The Third Affiliated Hospital of Guangzhou University of Chinese Medicine, No. 263, Longxi Avenue, Guangzhou, China
[4]Key Laboratory of Chinese Medicinal Resource from Lingnan (Guangzhou University of Chinese Medicine), Ministry of Education, Guangzhou, China
[5]State Key Laboratory of Dampness Syndrome of Chinese Medicine, Guangzhou University of Chinese Medicine, Guangzhou, China
[6]These authors contributed equally
[7]Lead contact
*Correspondence: jinhl@gzucm.edu.cn (H.-L.J.), wanghongbin@gzucm.edu.cn (H.-B.W.)
https://doi.org/10.1016/j.celrep.2023.112268

SUMMARY

The coordination of chloroplast and nuclear genome status is critical for plant cell function. Here, we report that *Arabidopsis* CHLOROPLAST AND NUCLEUS DUAL-LOCALIZED PROTEIN 1 (CND1) maintains genome stability in the chloroplast and the nucleus. CND1 localizes to both compartments, and complete loss of CND1 results in embryo lethality. Partial loss of CND1 disturbs nuclear cell-cycle progression and photosynthetic activity. CND1 binds to nuclear pre-replication complexes and DNA replication origins and regulates nuclear genome stability. In chloroplasts, CND1 interacts with and facilitates binding of the regulator of chloroplast genome stability WHY1 to chloroplast DNA. The defects in nuclear cell-cycle progression and photosynthesis of *cnd1* mutants are respectively rescued by compartment-restricted CND1 localization. Light promotes the association of CND1 with HSP90 and its import into chloroplasts. This study provides a paradigm of the convergence of genome status across organelles to coordinately regulate cell cycle to control plant growth and development.

INTRODUCTION

Chloroplasts in plants and algae have an endosymbiotic origin: over 2 billion years ago, a photosynthetic cyanobacterium-like organism was stably engulfed by a heterotrophic unicellular eukaryote.[1] This initial event was followed over the course of evolution by massive gene transfer from the green prokaryote genome to the host-cell nucleus, leading to the complete dependency of the endosymbiont on its surrounding cells and the generation of a novel type of organism, photosynthetic eukaryotes.[2] The development of higher plants requires the tight coordination of chloroplast development from undifferentiated proplastids in meristematic cells or from etioplasts, which differentiate from proplastids when seeds germinate in darkness. In addition to being the site of photosynthesis in leaf mesophyll cells, chloroplasts house essential metabolic pathways and contribute to storage and pigmentation in specialized cells.[3]

Eukaryote genomes are organized into multiple chromosomes whose replication initiates from numerous origins and is strictly regulated.[4] To maintain genome integrity and stability, genomic DNA must be replicated completely and accurately, but also only once during the S phase of the cell cycle. The formation of a pre-replication complex (pre-RC) is required for the subsequent ordered assembly of replication factors such as the Origin Recognition Complex (Orc), Cell Division Cycle6 (Cdc6) in budding yeast (*Saccharomyces cerevisiae*) or its ortholog CDC18 in fission yeast (*Schizosaccharomyces pombe*), chromatin licensing and DNA replication factor 1 (CDT1), and Mini Chromosome Maintenance (MCM) proteins (MCM2–7).[5] MCM proteins are essential replication initiation factors that were originally identified as proteins required for minichromosome maintenance, plasmid replication, or cell-cycle progression in yeast.[6] Indeed, cell-cycle checkpoints are crucial for genome integrity, as they stop cell-cycle progression upon DNA damage until repairs have been completed. Such mechanisms are particularly important in plants, which endure daily exposure to DNA-damaging agents such as light and reactive oxygen species (ROS).[7]

Although the mechanisms underlying nuclear genome maintenance are well understood, much less is known about the mechanisms that ensure chloroplast genome stability. Only a few factors involved in the maintenance chloroplast genomes in the model plant Arabidopsis (*Arabidopsis thaliana*) have been identified, among which the WHIRLY (WHY) proteins, a family of

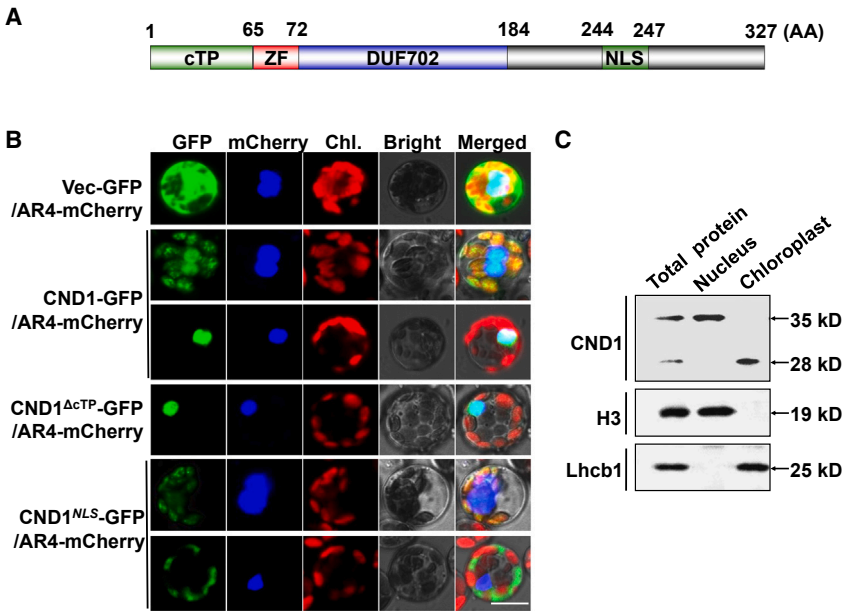

Figure 1. CND1 localizes to nuclei and chloroplasts

(A) Schematic diagram of CND1 showing the chloroplast transit peptide (cTP), Zinc Finger (ZF), domain of unknown function 702 (DUF702), and nuclear localization sequence (NLS).

(B) Subcellular localization of CND1-GFP fusions. Vec-GFP, control with empty vector; CND1-GFP, CND1-GFP fusion; CND1$^{\Delta cTP}$, CND1 lacking the cTP; CND1$^{\Delta NLS}$, CND1 lacking the NLS; AR4-mCherry, nuclear marker. Scale bars, 10 μm. Three biological replicates were performed.

(C) Subcellular localization of CND1 determined by immunolocalization analysis. Intact chloroplasts and nuclei fractions were isolated from Arabidopsis plants. Immunoblots were performed with polyclonal antibodies against CND1, light harvesting complex II subunit b (Lhcb1), and Histone H3 (H3). Two additional independent biological replicates were performed with similar results.

single-stranded DNA-binding proteins that guard organelles against genomic rearrangements.[8] WHYs have been proposed to stabilize single-stranded DNA and guide it through conservative repair mechanisms such as homologous recombination.[9] WHYs are present in all plant organelles; in Arabidopsis, WHY1 and WHY3 are targeted to chloroplasts, whereas WHY2 is targeted to mitochondria.[10] In addition, the RecA family of DNA-binding proteins promotes organellar genome stability through its central role in homologous recombination. Organelles contain three RecA proteins: chloroplast-localized RecA1, mitochondrion-targeted RecA3, and RecA2 targeted to both organelles.[11] A mutation in Arabidopsis DNA polymerase I B (Poll B) causes replication stress at early developmental stages and increases the number of double-strand breaks (DSBs) upon genotoxic stress.[12] Importantly, *polIB* and *recA* mutants exhibit a genetic interaction with *why* mutants in terms of DSB repair and maintenance of chloroplast genome structure.[13]

Coordination between the chloroplast and nuclear genomes is essential for sustaining photosynthesis, plant growth, and development.[14–17] Orchestrated gene expression between the chloroplast and nuclear genomes has been extensively studied.[18] Most regulators of chloroplast gene expression are encoded by nuclear genes.[19–22] However, chloroplast-to-nucleus retrograde signaling also integrates chloroplast function, including gene expression, photosynthetic electron transport, and redox state, to regulate nuclear gene expression, largely at the transcriptional level.[23] In recent years, several studies have reported the modulation of other aspects of nuclear function by the chloroplast, including post-transcriptional regulation via alternative splicing of RNA,[24] endoreplication, and cell-cycle progression.[25,26] However, the exact nature of the mechanism(s) coordinating genome stability between the chloroplast and the nucleus remains largely unknown.

In this study, we identified Arabidopsis CHLOROPLAST AND NUCLEUS DUAL-LOCALIZED PROTEIN 1 (CND1), which plays roles in the maintenance of genome stability in the chloroplast and the nucleus. Genetic analysis demonstrated that CND1 is required for photosynthesis, growth, and development. In the nucleus, CND1 binds to the pre-RC and origins of DNA replication, regulating DNA replication and the cell cycle. In the chloroplast, CND1 interacts with WHY1 and facilitates its association with chloroplast DNA. These findings suggest that CND1 functions in the stability of nuclear and chloroplast genomes.

RESULTS

CND1 is a nucleus and chloroplast dual-localized protein

To understand the functional coordination between the chloroplast and nucleus, we systematically screened proteins with predicted chloroplast and nucleus dual localization by combining bioinformatics and proteomics analyses. We focus here on one such putative chloroplast and nucleus dual-localized protein, encoded by the nuclear gene *At1g32730* that we named CHLOROPLAST AND NUCLEUS DUAL-LOCALIZED PROTEIN 1 (CND1). CND1 contains four predicted functional domains: two targeting domains, consisting of an N-terminal chloroplast transit peptide (cTP) (amino acids [aa] 1–65) based on TargetP prediction[27] and a nuclear localization sequence (NLS) containing the amino acid motif KRKK[28]; a zinc finger domain (ZF); and the domain of unknown function DUF702 (Figure 1A).

The presence of the cTP and NLS domains suggested that CND1 localizes to both chloroplast and nuclear compartments. To test this possibility, we determined the subcellular localization of full-length CND1 tagged with the green fluorescent protein (GFP) in Arabidopsis protoplasts by confocal laser scanning microscopy. We detected fluorescence from CND1-GFP in the nucleus and chloroplasts, demonstrating that CND1 is indeed a dual-localized protein. However, we noticed that the fluorescence signal often emanated from the nucleus alone, with only

a subset of protoplasts exhibiting fluorescence in both locations. Further analysis detected CND1-GFP signal only in the nucleus of cells with one nucleus, but from both the nucleus and chloroplasts in cells with two nuclei or more, as evidenced by co-localization with the nuclear marker AR4-mCherry (Figure 1B). Furthermore, we established that the NLS is required for nuclear localization, as mutating the NLS motif from KRKK to KLNQ eliminated the accumulation of CND1^{mNLS}-GFP in the nuclei when the cell contained two nuclei, and restricted CND1^{mNLS}-GFP accumulation to the cytoplasm and chloroplasts when there was one nucleus (Figure 1B). Likewise, the deletion of the cTP resulted in the exclusive nuclear localization of CND1$^{\Delta cTP}$-GFP (Figure 1B). Our results show that CND1 localizes to chloroplasts and nuclei when there are two nuclei in one cell, and mainly to the nucleus when there is one nucleus in the cell.

To validate these observations, we raised a specific anti-CND1 antibody and determined the subcellular localization of endogenous CND1 by immunoblot analysis of total leaf protein extracts. The antibody recognized two bands with different molecular weights: one species of about 35 kDa, and one of about 28 kDa (Figure 1C). Full-length CND1 has a predicted molecular weight of 36 kDa; however, the cTP signal consists of 65 amino acids, which would result in a mature chloroplast-localized protein of about 28 kDa after import into the organelle and cleavage of the cTP signal. To test this prediction, we prepared nuclear and chloroplast fractions from wild-type Arabidopsis plants. Immunoblot analysis of these fractions indicated that the 35-kDa form of CND1 accumulates exclusively in the nucleus, while the 28-kDa form of CND1 was specific to the chloroplast fraction (Figure 1C). We also confirmed the specificity of the CND1 antibody in lines expressing a *CND1-Flag* construct (Figure S1A). These results indicate that CND1 is a nucleus and chloroplast dual-localized protein.

Mutations in CND1 lead to embryo lethality and abnormal development

To explore the role of CND1 during plant development, we obtained two independent transfer DNA insertion lines from the SALK collection, hereafter referred to as *cnd1-1* and *cnd1-2* (Figure 2A). We screened seedlings by PCR and identified only *cnd1/CND1* hemizygous and wild-type plants in a 2:1 ratio (n = 76), indicating that homozygous *cnd1* plants are not viable. Indeed, siliques from *cnd1-1/CND1* and *cnd1-2/CND1* plants contained 23% ± 5% and 26% ± 3% aborted seeds (Figure 2B), respectively, consistent with an expected segregation of 25% of homozygous *cnd1-1* and *cnd1-2* seeds. These results suggest that disruption of *CND1* is embryo lethal.

To investigate at which stage of embryogenesis *cnd1* mutants arrested, we studied embryo development in *cnd1/CND1* siliques; both alleles gave identical results. In the same silique, we observed embryos at different developmental stages: 75% of embryos reached the globular stage, while 25% remained at the pre-globular stage. By the time wild-type and hemizygous embryos had reached the late heart stage, homozygous *cnd1* embryos did not develop further (Figure 2C). We also examined the development of the embryo sac and pollen and found that pollen and embryo sac development was normal (Figure S2). We therefore conclude that loss of CND1 function causes a recessive sporophytic seed-lethality phenotype at a very early stage of embryogenesis, thus providing evidence for an essential role for CND1 during embryo development.

Since they were embryo lethal when homozygous, the *cnd1-1* and *cnd1-2* null mutations were not useful for characterizing the role of CND1 during plant growth and development. However, we also isolated a *CND1* knockdown allele, subsequently named *cnd1-3*, which allowed plants to reach maturity in the homozygous state (Figure 2A). *CND1* expression in *cnd1-3* mutant plants was ~27% of that in wild-type plants (Figure 2D), which was consistent with decreased full-length CND1 and CND1$^{\Delta cTP}$ protein accumulation in the *cnd1-3* mutant (Figure S1B). *cnd1-3* plants had narrower leaves than the wild type, with markedly serrated margins (Figure 2E). To confirm that this phenotype was due to *CND1* downregulation, we also generated *CND1* RNA interference (RNAi) transgenic lines, in which *CND1* expression decreased to 24% (in the *CND1*-RNAi #22 line) and 19% (in the *CND1*-RNAi #26 line) of wild-type levels (Figure 2D), which was also consistent with decreased full-length CND1 and CND1$^{\Delta cTP}$ protein accumulation in the *cnd1-3* mutant (Figure S1B). These RNAi lines displayed the same phenotypes as *cnd1-3* plants, including narrower and serrated leaves, as well as slower growth (Figure 2E). The average leaf epidermal cell area was larger in *cnd1-3*, *CND1*-RNAi #22 and *CND1*-RNAi #26 plants compared with the wild type (Figure 2F). These results suggest that downregulation of *CND1* results in abnormal leaf development.

CND1 associates with the Pre-RC and origins of DNA replication in the nucleus

To delineate how CND1 regulates plant growth and development, we identified genes that are co-expressed with *CND1* from the ATTED II database. Notably, *CND1* was co-expressed with genes encoding multiple members of the DNA pre-RC, including MCM proteins, CDT1, DNA polymerase, and REPLICATION PROTEIN A (RPA) proteins (Figure S3A), indicating that CND1 might be involved in the regulation of DNA replication. Considering the nuclear distribution of CND1, we tested the physical interaction of CND1 and these pre-RC proteins by bimolecular fluorescence complementation (BiFC) assays. We observed strong interaction between CND1 and multiple members of the DNA pre-RC, which all participate during the early stages of DNA replication initiation: MCM2-5, CDT1A/B, and CYCLIN D5; 1 (CYCD5; 1) (Figures S3B and 3A). However, we did not detect a clear interaction between CND1 and the RPA proteins RPA70B/D, or DNA POLYMERASE DELTA 3 (POLD3), which function during later stages of DNA replication initiation. These results suggest that CND1 is associated with the early pre-RC. Yeast two-hybrid (Y2H) assays showed that CND1 specifically interacts with MCM4, but not with other pre-RC proteins (Figures 3B and S3C), suggesting that CND1 associates with the pre-RC via direct interaction with MCM4. The N terminus of MCM proteins contains a ZF motif, which represents the largest class of eukaryotic transcription factors and DNA-binding motifs. The ZF motif is typically involved in DNA-protein or protein-protein interactions.[5] As noted earlier, CND1 also contains a ZF motif, prompting us to test whether CND1 interacted with MCM4 via their respective ZF domains. CND1 lacking the ZF motif failed to interact with

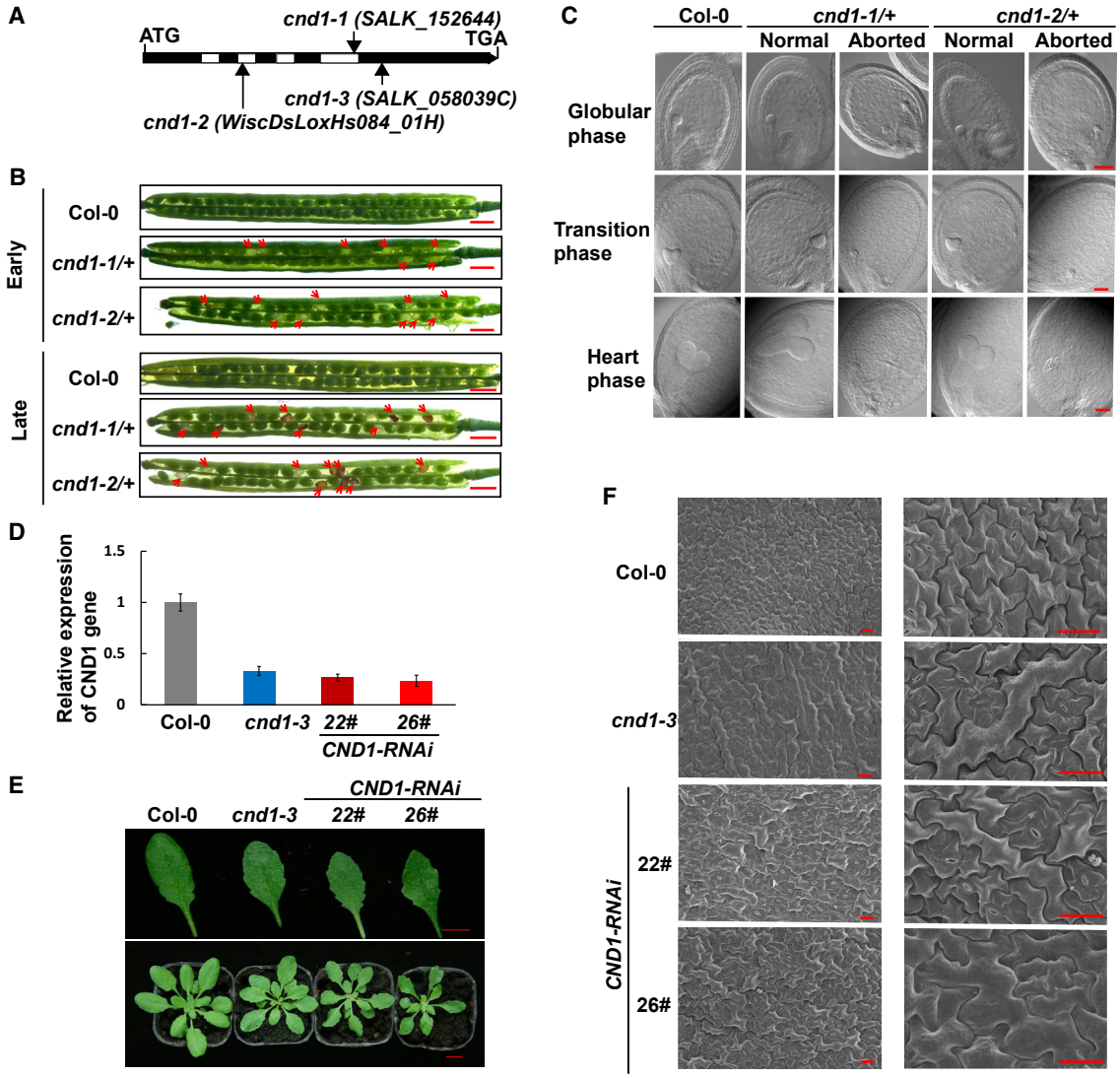

Figure 2. Loss of CND1 function results in embryo lethality and abnormal development

(A) Schematic diagram of *CND1* inferred by DNA sequence analysis. Exons (black boxes) and introns (white boxes) are indicated. The positions of the transfer DNA insertions corresponding to the *cnd1-1*, *cnd1-2,* and *cnd1-3* mutants are shown. ATG start codon and TGA stop codon are shown.

(B) Fully developed siliques from wild-type (Col-0), *cnd1-1*/+, and *cnd1-2*/+ plants were opened and observed using a microscope. Red arrows point to aborted ovules. Scale bars, 1 mm.

(C) Development of embryos in siliques from wild-type (Col-0), *cnd1-1*/+, and *cnd1-2*/+ plants. Images show embryos at the pre-globular stage, embryos at the globular stage, and embryos at the heart stage. Scale bars, 50 μm.

(D) RT-qPCR analysis of *CND1* transcript levels in wild-type plants, *cnd1-3,* and *CND1*-RNAi (*CND1*-RNAi #22 and #26) lines. The transcript level of each gene was normalized relative to *ACTIN2* (At3g18780).

(E) Representative images of leaf phenotypes of 4-week-old wild-type plants, the *cnd1-3* mutant, and *CND1*-RNAi lines (*CND1*-RNAi #22 and #26). Values are means ± SE, n = 3 independent biological replicates.

(F) SEM of the leaf lower epidermis of wild-type, *cnd1-3* and *CND1*-RNAi (*CND1*-RNAi #22 and #26) plants. Over 20 independent biological replicates were performed in all experiments, with similar results.

MCM4 in BiFC or Y2H assays (Figures 3A and 3B), indicating that CND1 interacts with MCM4 via its ZF motif. We corroborated the interaction of CND1 and MCM4 by a co-immunoprecipitation (coIP) assay (Figure 3C).

We tested whether CND1 associates with nuclear DNA using chromatin immunoprecipitation followed by deep sequencing (ChIP-seq). The data of two biological replicates of ChIP-seq were highly reproducible and of high quality (Table S1). We identified 2,558 association sites for CND1 across the nuclear genome (Figure 3D; Table S2). CND1 associated with intragenic regions (promoters, 5′ untranslated regions [5′ UTRs], 3′ UTRs, introns, and exons of genes), and intergenic

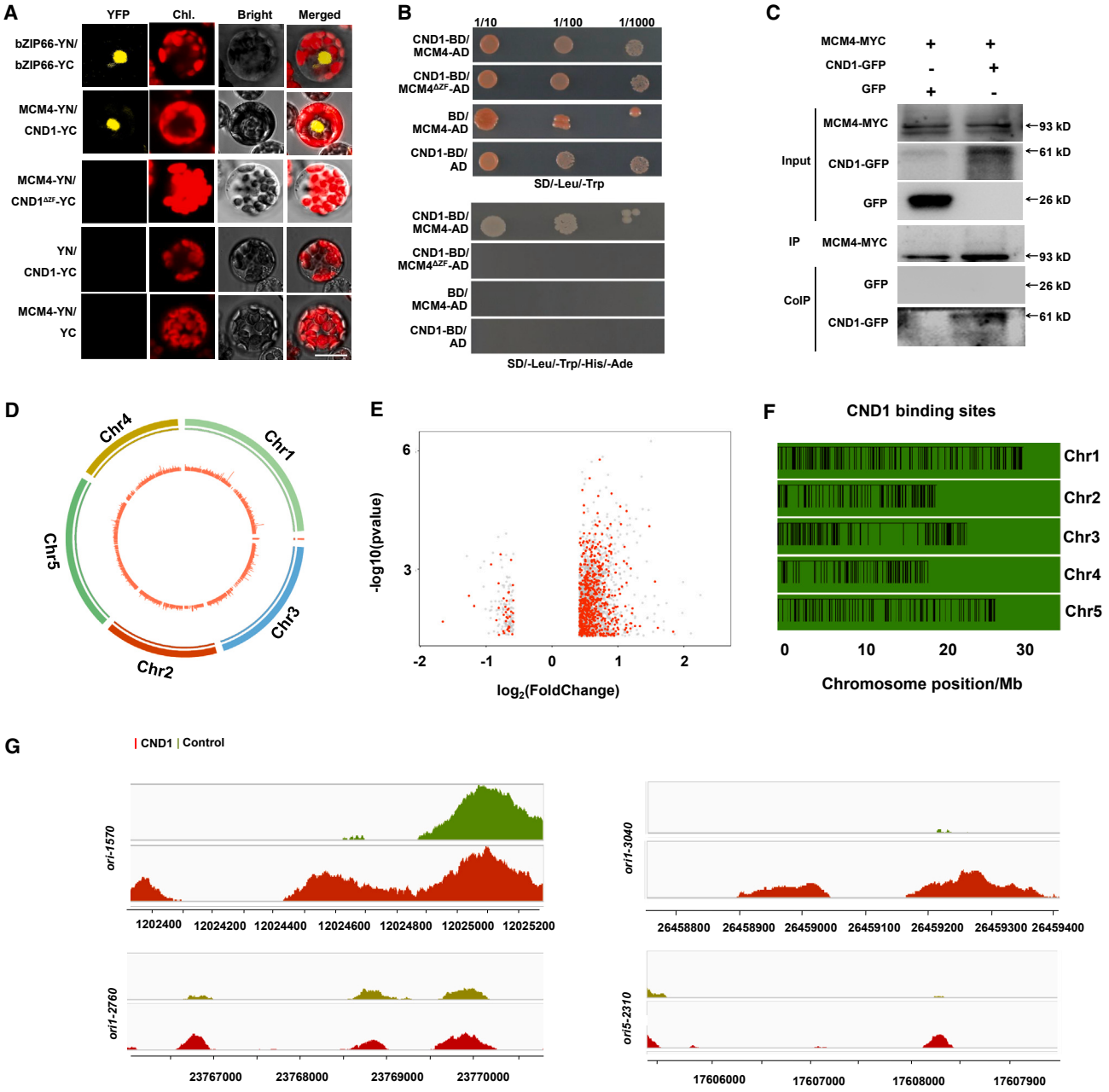

Figure 3. CND1 interacts with the DNA pre-replication complex and origins of DNA replication in the nucleus

(A) Interaction of CND1 with the pre-replication complex protein MCM4 by BiFC analysis. CND1-YC and MCM4 or MCM4$^{\Delta ZF}$-YN were co-transfected into Arabidopsis protoplasts and visualized by confocal microscopy. bZIP66-YN and bZIP66-YC were used as positive control. CND1-YC+YN and MCM4-YN+YC were used as negative control. Scale bars, 10 μm.

(B) Y2H assays confirming that CND1 interacts only with MCM4. CND1 or CND1$^{\Delta ZF}$-BD and MCM4-AD were co-transformed into yeast. CND1-BD/AD and MCM4-AD/BD were used as negative control.

(C) MCM4-YN was allowed to accumulate for 12 h in protoplasts isolated from *CND1-GFP* transgenic lines and visualized by coIP.

(D) Quantitative association of CND1 with DNA as measured by ChIP-seq. Genome browser views show the distribution of sites associated with statistically significant CND1 binding across the nuclear genome.

(E) Volcano plot of all CND1-binding genes in ChIP-seq (gray and blue) and extent of overlap with DNA replication origins (blue). The CND1-bound genes were obtained from the ChIP-seq data of CND1-Flag in the *cnd1-3* mutant compared with Col-0, and CND1-bound genes associated with origins of DNA replication were identified by comparing the statistically significant changed CND1-binding genes with the fraction of DNA replication origins.

(F) Genome browser views showing the distribution of sites associated with CND1 binding across the nuclear genome that matched to origins of DNA replication.

(legend continued on next page)

regions (distal intergenic regions and proximal downstream regions) (Figures S3D and S3E). Because DNA pre-RCs bind to origins of DNA replication to regulate the initiation of DNA replication and the cell cycle, we assessed the extent of CND1 association to the origins of DNA replication. We determined that CND1 associates with 673 origins of DNA replication (Figure 3E; Table S3); the distribution of DNA replication origins associated with CND1 across the nuclear genome is shown in Figure 3F, such as ori-1570, ori1-2760, ori1-3040, and ori5-2310 (Figure 3G),[29–31] suggesting that CND1 associates with origins of DNA replication. We asked whether the CND1-pre-RC interaction has functional consequence on MCM4 DNA binding by measuring the association of MCM4 to DNA replication origins in the wild-type and *cnd1-3* backgrounds by ChIP-qPCR using an anti-FLAG antibody. The association of MCM4 with origin sites of DNA replication decreased in the *cnd1-3* mutant at all sites tested, but not at a control locus not containing an origin site (Figure S3F). These results suggest that CND1 interacts with MCM4 and facilitates the association of MCM4 with nuclear DNA.

In addition, Gene Ontology (GO) analysis indicated CND1 associated with genes related to "cell cycle and DNA metabolism," "post-embryonic development," and "response to stress" (Figure S3G). We also performed transcriptome deep sequencing (RNA-seq) to compare gene expression patterns between *cnd1-3* and wild-type plants (Table S4). GO analysis showed that significant differentially expressed genes (DEGs) in the mutant are enriched in biological processes related to DNA damage and repair, and response to stress (Figure S4A; Table S4). Furthermore, GO analysis of the overlap genes from ChIP-seq and RNA-seq data showed that they are also enriched in many DNA replication and DNA damage and repair (DDR) genes involving in biological processes of response to endogenous stimulus, reproduction, post-embryonic development, and DNA metabolism process (Figures S4B and S4C). These results suggest that CND1 is also involved in regulating DNA replication and DDR genes.

CND1 is required for maintenance of nuclear genome stability

The members of the pre-RC regulate the cell cycle and genome stability.[7,32,33] To test whether CND1 functions in the cell cycle and genome stability, we monitored the expression of several genes involved in DNA repair pathways in wild-type and *cnd1-3* homozygous plants; the expression of *Ku70*, *POLY(ADP-RIBOSE) POLYMERASE 2* (*PARP2*), *RADIATION SENSITIVE 51* (*RAD51*), *BREAST CANCER TYPE 1* (*BRCA1*), and *X-RAY CROSS-COMPLEMENTATION 4* (*XRCC4*) was higher in *cnd1-3* plants relative to wild type (Figure 4A), indicative of possible increased DNA instability. This result provided evidence for endogenous DNA stress induced by lower CND1 function. Next, we compared the DNA content of *cnd1-3* and wild-type plants by flow cytometry analysis. Wild-type leaves typically show nuclei with a 2C–16C DNA content, with a majority of 2C, 4C, and 8C nuclei and only a few 16C nuclei. By contrast, the bulk of nuclei in *cnd1-3* plants and *CND1*-RNAi lines had a higher proportion of 8C and 16C nuclei (Figures 4B and 4C). Therefore, DNA appears to have undergone one additional round of replication in *cnd1-3* plants and *CND1*-RNAi lines relative to the wild type. These results suggest that CND1 is required for maintenance of nuclear genome stability.

DNA methylation modifications contribute to genome stability in multiple ways.[34,35] The *cnd1-3* mutant showed an altered DNA methylation profile when compared with the wild type, as determined by methylated DNA immunoprecipitation followed by deep sequencing (MeDIP-seq) (Figures 4D and S4D). Compared with wild-type plants, we identified 55,476 significantly downregulated peaks of DNA methylation covering 8,664 genes and 131,125 significantly upregulated peaks of DNA methylation covering 15,353 genes in *cnd1-3* plants (Figure 4E; Table S6). Notably, 4,360 differential peaks of DNA methylation overlapped with origins of DNA replication, of which 473 were bound by CND1 (Figure 4F; Table S3). In addition, 14 differential peaks of DNA methylation overlapped with cell cycle- and genome stability-related genes, of which 12 genes were bound by CND1, such as *MCM3*, *SISTER CHROMATID COHESION 1 (SCC1) PROTEIN HOMOLOG 2* (*SYN2*) RADIATION SENSITIVE 17 (*RAD17*), and *UV HYPERSENSITIVE 1* (*UVH1*) (Table S5). These results indicate that the partial loss of CND1 function affects DNA methylation levels of origins of DNA replication, as well as the cell cycle and genome stability.

CND1 plays a role in maintenance of chloroplast genome stability

The localization of CND1 in chloroplasts suggested that CND1 also had roles in this organelle. To determine whether CND1 plays a similar role in the maintenance of genome stability in chloroplasts, we measured the plastid DNA content in wild-type and *cnd1-3* plants by flow cytometry. The plastid DNA content was higher in the *cnd1-3* mutant than in wild-type plants (Figure 5A), a result quantitatively similar to our initial observations of *cnd1-3* nuclear DNA content (Figure 4B). Genome maintenance in chloroplasts is tightly controlled by many proteins acting in concert to repress the accumulation of DNA rearrangements. Genome instability results in increased DNA rearrangements largely driven by higher recombination between short direct repeats scattered across the chloroplast genome. We tested the extent of genome instability in wild-type and *cnd1-3* plants by taking an outward-facing PCR approach according to a previous study.[8] We performed this analysis on two independent DNA pools from wild-type and *cnd1-3* plants. Representative results of the PCR amplification are shown in Figure 5B. Cloning and sequencing of rearranged DNA confirmed the strong rise in illegitimate recombination in *cnd1-3* plants relative to the wild type. However, we also detected rearranged products in wild-type plants, suggesting the presence of a small

(G) Enlarged regions containing a replication origin. Origins, e.g., ori1-1570 shown here, are named based on their chromosomal location (ori1, chromosome 1 and ori5, chromosome 5) followed by the four digits that indicate the origin number within each chromosome, according to genome-wide mapping of Arabidopsis origins of DNA replication.[29–31] Two independent biological replicates were performed for the ChIP-seq, and other experiments were performed three times.

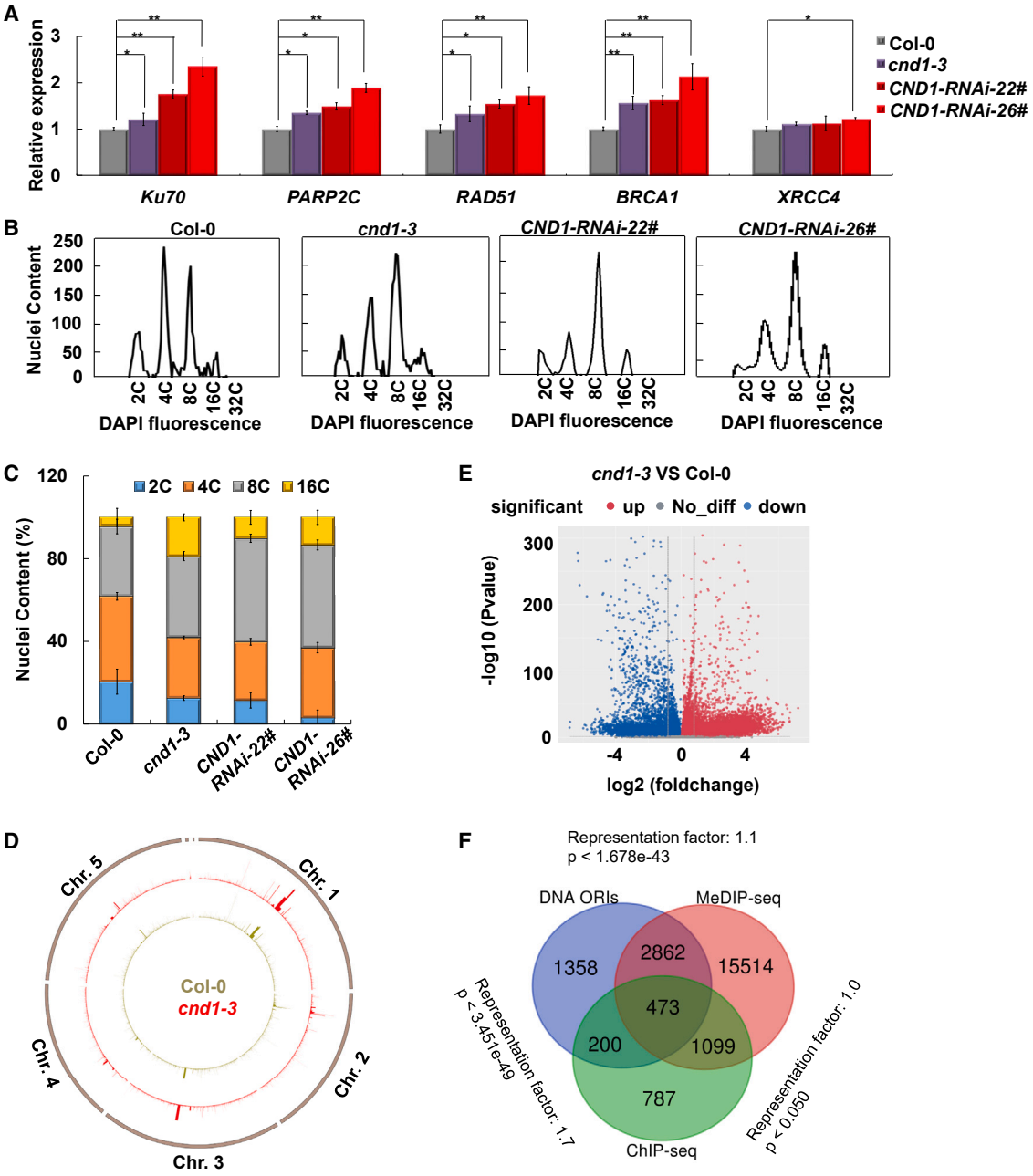

Figure 4. The role of CND1 in maintenance of nuclear genome stability

(A) Expression of genes involved in DNA repair pathways, as determined by RT-qPCR, in wild-type (Col-0), *cnd1-3,* and *CND1*-RNAi (*CND1*-RNAi #22 and #26) plants. The transcript level of each gene was normalized relative to *ACTIN2* (At3g18780). Data presented here represent two biological replicates. Each RT-qPCR was repeated at least twice on each biological replicate (*$p < 0.05$, **$p < 0.01$; Student's t test).

(B) Analysis of nuclear DNA content in wild-type, *cnd1-3,* and *CND1*-RNAi (*CND1*-RNAi #22 and #26) plants. Nuclei were isolated and their DNA content analyzed by flow cytometry after staining with DAPI. DNA content was measured in at least 6,000 nuclei isolated from the first leaf of seedlings harvested 14 days after release from stratification. Three independent biological replicates were performed.

(C) Quantitative analysis of DNA ploidy shown in (B).

(D) Analysis of nuclear DNA methylation profiles in wild-type and *cnd1-3* plants ($p < 0.05$, Fold-Change >2).

(E) Volcano plot of DNA methylation profiles in *cnd1-3* compared with wild-type plants. The outside circle represents chromosome 1 to chromosome 5 in Arabidopsis.

(F) Venn diagram displaying the overlap among differentially methylated genes in *cnd1-3* and Col-0 ($p < 0.05$, Fold-Change>2), the p values and representation factors between two data were calculated by hypergeometric tests, the CND1-bound genes from all peaks in CND1-Flag in the *cnd1-3* mutant compared with Col-0 by ChIP-seq, and all DNA replication origins (ORIs) identified in previous studies.[29–31]

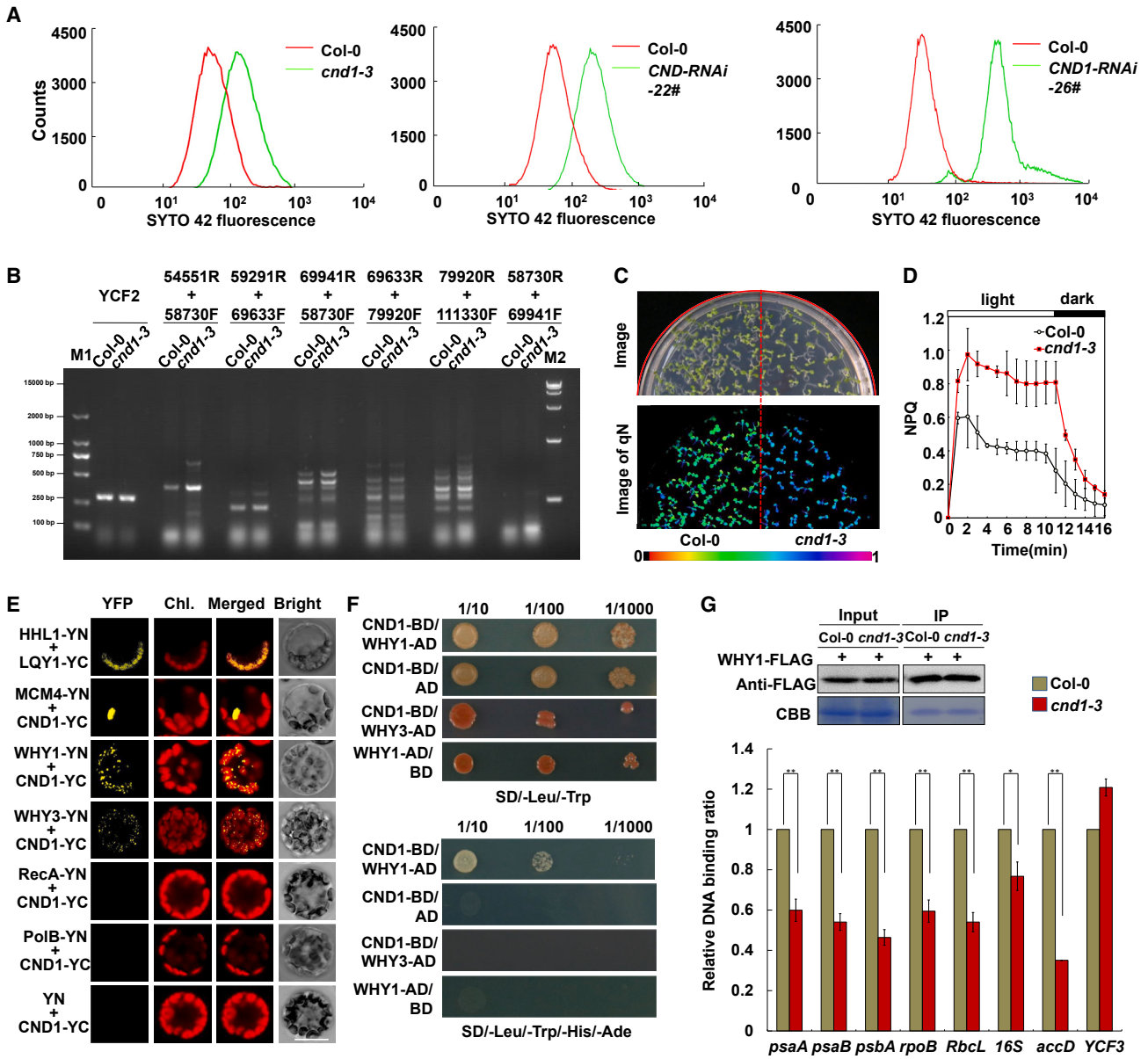

Figure 5. Role of CND1 in maintenance of chloroplast genome stability

(A) Chloroplast DNA content in wild-type, *cnd1-3,* and *CND1*-RNAi (*CND1*-RNAi #22 and #26) plants. Chloroplasts were isolated and their DNA content analyzed by flow cytometry using the SYTO 42 fluorescent dye.

(B) Analysis of illegitimate recombination in the chloroplast genome in wild-type, *cnd1-3,* and *CND1*-RNAi (*CND1*-RNAi #22 and #26) plants. For each genotype, PCR reactions using outward- or inward-facing PCR primers were performed on seven pools of DNA from seven different plants.

(C) Analysis of non-photochemical quenching, as determined by chlorophyll fluorescence imaging in wild-type and *cnd1-3* plants.

(D) Non-photochemical quenching kinetics, measured as chlorophyll fluorescence kinetics.

(E) Interaction between CND1 and chloroplast genome stability regulators by BiFC assay. CND1-YC and WHY1, WHY3, RecA, or PolI B-YN were co-transfected into Arabidopsis protoplasts and visualized by confocal microscopy. HHL1-YN and LQY1-YC were used as positive control.[36] CND1-YC +YN were used as negative control. Scale bars, 10 μm.

(F) Y2H assays confirming that CND1 interacts only with WHY1. CND1-BD and WHY1, WHY3, RecA, or PolI B-AD were co-transformed into yeast. CND1-BD/AD and WHY1-AD/BD were used as negative control.

(G) Effect of decreased CND1 function on the association of WHY1 with chloroplast DNA. The y axis represents the amount of DNA that co-immunoprecipitated with WHY1 in the *cnd1-3* mutant compared with the amount in the wild type (Col-0) by qPCR. The gene region of *Ycf3* was used as a negative control[9] (*$p < 0.05$, **$p < 0.01$; Student's t test). Wild-type levels were set to 1. Three independent biological replicates were performed for all experiments.

subpopulation of rearranged chloroplast DNA even under normal physiological conditions. These results support a role for CND1 in chloroplast genome stability.

Since photosynthesis occurs in chloroplasts, we determined if the downregulation of *CND1* expression affected chloroplast size; however, chloroplast size was unchanged in the *cnd1-3* mutant (Figures S5A–S5D). We also determined photosynthetic capacity by examining chlorophyll fluorescence parameters in *cnd1-3* and wild-type plants. We did not detect obvious differences for maximum photochemical quenching (*Fv*/*Fm*) between the two genotypes (Figure S5E); heat dissipation by non-photochemical quenching (NPQ) was higher in the *cnd1-3* mutant compared with the wild type in normal growth light conditions (Figures 5C and 5D). Carotenoids are pigments that modulate photosynthetic light harvesting and photoprotection.[37] BiFC assays revealed that CND1 interacts with key enzymes of the xanthophyll cycle, NPQ1 and NPQ2, required for NPQ (Figure S5F), although the composition of carotenoids was not affected in the *cnd1-3* mutants (Figure S5G).

Plastid genome instability results in ROS bursts.[38] We thus examined the levels of O^{2-}, H_2O_2, $^1O_2$, and total ROS in *cnd1-3* mutants according to the methods of our previous study.[36] The levels of O^{2-}, H_2O_2, $^1O_2$, and total ROS are increased in *cnd1-3* compared with wild-type plants (Figures S5H–S5K). We examined the effect of oxidative stress from ROS on the abundance of photosynthetic complexes in *cnd1-3*. To this end, we solubilized thylakoid membranes in 2% dodecyl maltoside, separated membrane protein complexes by blue native (BN)-polyacrylamide gel electrophoresis (PAGE) (Figure S5L), and analyzed the complexes by immunoblotting with antibodies specific for photosystem II (PSII) core proteins. Results with anti-D1 antibody showed that the *cnd1-3* mutant contains less PSII-light harvesting complex II (LHCII) supercomplexes than wild-type thylakoid membranes (Figure S5L). We also detected lower levels of the PSII core subunits D2, CP43 and CP47 in the *cnd1-3* mutant (Figures S5M and S5N). These results were based on an equal chlorophyll basis. By contrast, levels of PsbO (another PSII protein), the PSI proteins PsaA and PsaD, the light harvesting complex II (LHCII) chlorophyll *a*/*b* binding proteins LHCa1 and LHCb1, ATP synthase subunit B, and cytochrome *f* were relatively stable in both wild-type and mutant plants (Figures S5M and S5N). Taken together, these results suggest that compromised CND1 function perturbs the relative levels of PSII complexes and core subunits.

Several key regulators of chloroplast genome stability have been identified, such as WHY1, WHY3, RecA1, and POLIB.[13] As CND1 appears to regulate chloroplast genome stability in a manner similar to that of the nuclear genome, and because we measured higher DNA contents and more DNA recombination in the *cnd1-3* plastid genome than in the wild type, we explored a potential interaction between CND1 and other regulators of chloroplast genome stability by BiFC assays using an Arabidopsis protoplast transient transfection system. CND1 interacted with WHY1 and WHY3 in a BiFC assay (Figure 5E). However, CND1 only interacted with WHY1, but not WHY3, in a Y2H assay (Figure 5F), which we verified by a coIP assay (Figure S5O). WHYs bind to organellar DNA to maintain DNA stability.[9] To determine the function of the CND1–WHY1 interaction, we assessed the effect of diminished CND1 function in the *cnd1-3* mutant on the association of WHY1 with DNA by ChIP-qPCR. Indeed, the association of WHY1 with chloroplast DNA decreased in the *cnd1-3* mutant relative to the wild type at the plastid genes *psaA*, *psaB*, *psbA*, *rpoB*, *RbcL*, *16S,* and *accD*, but not the negative control *Ycf3* (Figure 5G). These results indicate that CND1 interacts with WHY1 to facilitate its association with chloroplast DNA.

A nucleus- or chloroplast-restricted localization of CND1 functionally rescues *cnd1* abnormal leaves or defected photosynthetic capacity

To understand how CND1 coordinates genome stability in chloroplasts and the nucleus, we analyzed the phenotypes associated with overexpressing chimeric variants of CND1 lacking the NLS, cTP, or ZF domains in the *cnd1-3* mutant background (Figures 6A, 6B, S6A, and S6B). Full-length CND1 rescued the abnormal chlorophyll fluorescence and serrated leaves phenotypes seen in the *cnd1-3* mutant. Versions of CND1 lacking either the NLS or the ZF domain also rescued the abnormal chlorophyll fluorescence phenotype, but not the leaf serration phenotype. The CND1 variant lacking the cTP failed to rescue the serrated leaves phenotype and abnormal chlorophyll fluorescence (Figures 6B and S6C).

We characterized the nuclear DNA content of these transgenic lines by flow cytometry analysis: full-length CND1 mostly restored the nuclear DNA ploidy profile to wild-type levels (Figures 6C and 6D). However, CND1 variants without the NLS, ZF, or cTP failed to rescue this phenotype (Figures 6C and 6D), suggesting that the complete CND1 protein is required for the maintenance of nuclear genome stability. Outward-facing PCR analysis showed that full-length CND1 and CND1 lacking either the NLS or the ZF domain rescue the abnormal DNA rearrangements detected in the chloroplasts of the *cnd1-3* mutant (Figure 6E). By contrast, the CND1 variant lacking the cTP did not protect chloroplast DNA from illegitimate recombination (Figure 6E), indicating that the localization of CND1 to chloroplasts is required for the maintenance of plastid genome stability.

CND1 exhibits dynamic expression and intracellular distribution patterns

We examined *CND1* expression across vegetative and floral development using reverse transcription quantitative PCR (RT-qPCR) (Figure 7A). *CND1* expression generally followed the same pattern as *CYCLIN B1;1* (*CYCB1;1*; Figure 7A), which encodes a B-type cyclin that is often used as a marker for cell proliferation.[39] *CND1* and *CYCB1;1* transcripts were most abundant in shoot apices and flower buds, which are rich in mitotic and endocycling cells.[40,41] We collected cell culture samples during the exponential growth stage based on *CYCB1;1* expression, which contained a comparable fraction of replicating cells as a microdissected shoot apical region. The lowest signals were detected in mature and senescing leaves (Figure 7A), consistent with the absence of DNA replication in these tissues. Together, these results demonstrate that *CND1* expression is developmentally regulated in Arabidopsis.

Because steady-state *CND1* transcript levels do not reflect the subcellular localization of the translated protein, we conducted

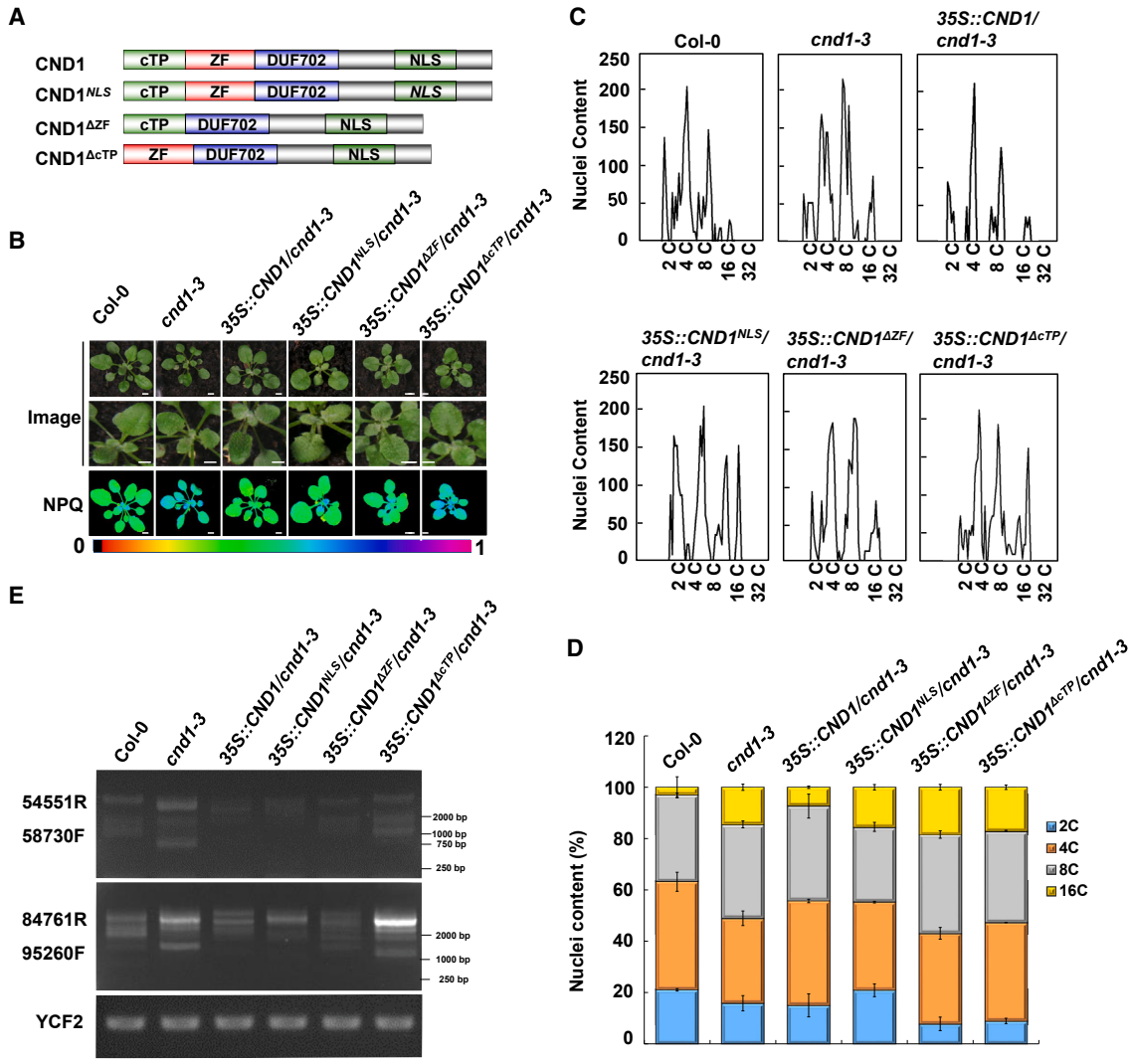

Figure 6. Physiological and molecular roles of different CND1 motifs

(A) Schematic diagram of CND1 variants lacking the chloroplast transit peptide (cTP), zinc finger (ZF), domain of unknown function 702 (DUF702), or carrying a mutated version of the nuclear localization sequence (NLS).

(B) Rescue tests of *cnd1-3* by the CND1 protein variants shown in (A) for leaf development and photosynthetic capacity. Bars = 0.5 cm.

(C) Rescue tests of *cnd1-3* by the CND1 protein variants shown in (A) on nuclear DNA ploidy by flow cytometry analysis.

(D) Quantification of DNA ploidy shown in (C).

(E) Rescue tests of *cnd1-3* by the CND1 protein variants shown in (A) on DNA rearrangements in the chloroplast genome by outward-facing PCR analysis. Three independent biological replicates were performed for all experiments.

an immunoblot analysis of various tissues: photosynthetically active mature leaves, the shoot apical meristem, and seeds. The size difference between nucleus- and chloroplast-localized CND1 in immunoblots provided a convenient assay to determine the fraction of CND1 in each compartment. In mature leaves, CND1 mainly localized to chloroplasts, with a small nuclear fraction (Figure 7B). In the shoot apex, CND1 localized prominently to the nucleus but with a substantial chloroplast fraction. In seeds, CND1 mainly localized to the nucleus, which is in agreement with the lack of developed chloroplasts in this tissue (Figure 7B). These results, combined with the results of dual localization in protoplast cells with two nuclei (Figure 1B), suggest that the genome stability of plastid and nucleus are more needed to coordinate when the cells are in the stage of division.

Considering the function of CND1 in chloroplasts and the absence of plastid-localized CND1 in seeds, we asked whether light affected CND1 accumulation and/or CND1 import to the chloroplast. We first established a system of light induction to control photosystem biogenesis in Arabidopsis: after 5 days of growth in the dark, we exposed etiolated seedlings to white light (100 μmol photons $m^{-2}s^{-1}$) for 4, 8, 12, 24, or 48 h. The leaves of wild-type seedlings gradually turned green when exposed to

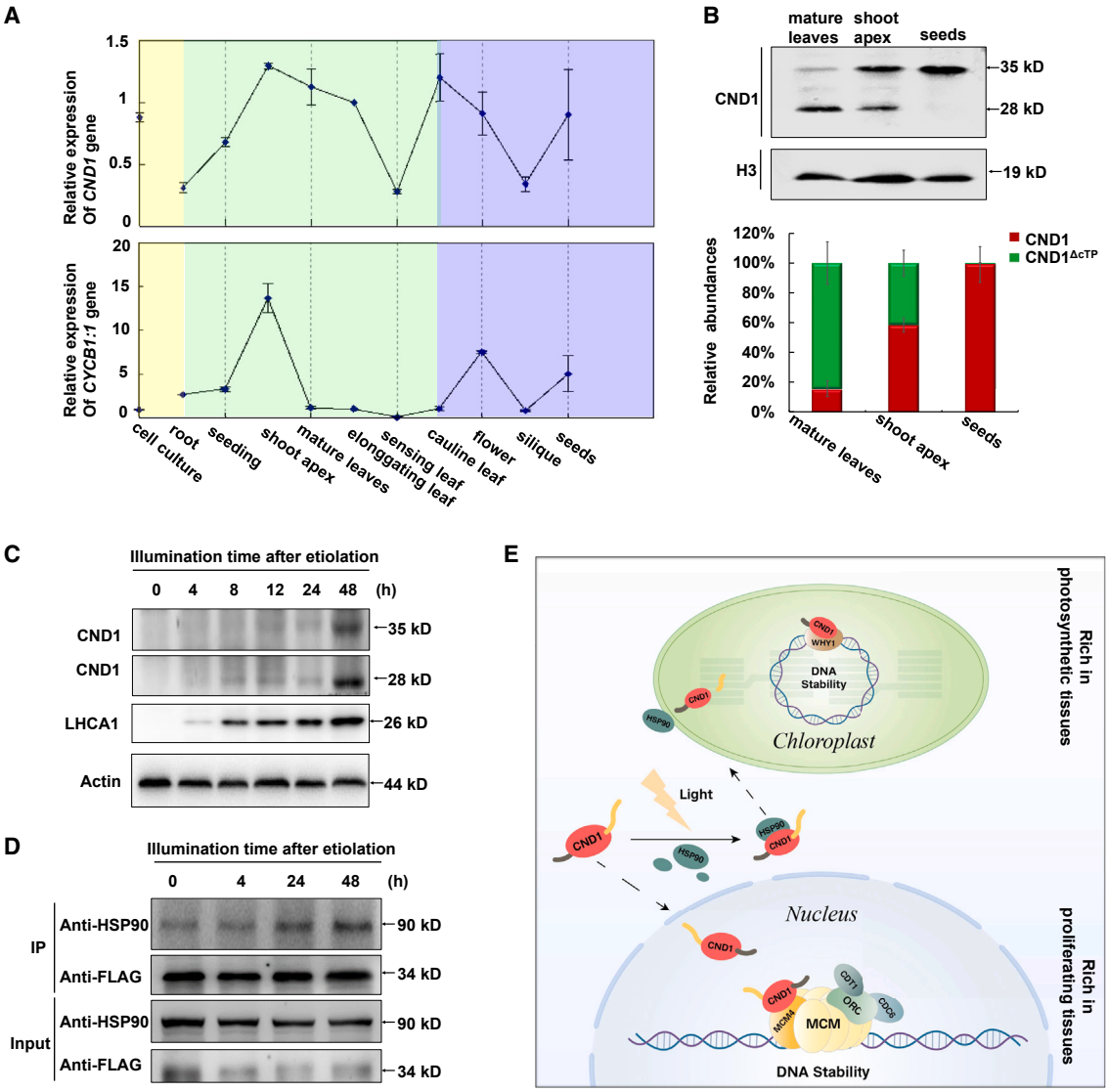

Figure 7. Dynamic distribution and import of CND1 into chloroplasts and the nucleus

(A) RT-qPCR analysis of *CND1* expression in Arabidopsis vegetative (shaded green) and floral (shaded blue) tissues and in suspension cell cultures (shaded yellow). The relative levels are scaled to expression in seedlings. *CYCB1;1* (At4g37490) was used as a marker for cell proliferation. The transcript level of each gene was normalized relative to *ACTIN2* (At3g18780).

(B) Subcellular distribution of CND1 in mature leaves, the shoot apex and seeds. The upper panel shows immunoblot analysis of different forms of CND1 in mature leaves, the shoot apex, and seeds. The lower panel shows the quantitative analysis of the signal in the upper panel.

(C) Accumulation of CND1 and LHCA1. After 5 days of growth in the dark, etiolated seedlings were exposed to white light (100 μmol photons $m^{-2}s^{-1}$) for 4, 8, 12, 24, or 48 h.

(D) Interaction of CND1 with HSP90. After 5 days of growth in the dark, etiolated seedlings were exposed to white light (100 μmol photons $m^{-2}s^{-1}$) for 4, 24, or 48 h. Three independent biological replicates were performed for all the experiments.

(E) Proposed working model of CND1 in maintenance of chloroplast and nucleus genome stability. CND1 is a chloroplast and nucleus dual-localized protein encoded by a nuclear gene. *CND1* mRNA is translated to CND1 protein by ribosomes in the cytoplasm. Driven by its N-terminal transit peptide, CND1 is target to chloroplasts, where it directly regulates genome stability by facilitating the association of WHY1 with chloroplast DNA. The nucleo-cytoplasmic partitioning of CND1 is controlled by its NLS motif. In the nucleus, CND1 physically interacts with the DNA pre-RC to promote nuclear genome stability. Full-length CND1 in the nucleus is mainly distributed in proliferating tissues, but mature CND1 without the cTP is mainly distributed in the chloroplasts of photosynthetic tissues. In addition, light promotes CND1 accumulation and its import into chloroplasts via association with the molecular chaperone HSP90.

increasing periods of illumination, with a concomitant increase of F_v/F_m and qN (Figure S7A), validating our experimental setup. *CND1* transcript and CND1 protein levels rose with longer exposure to light in the nucleus and chloroplasts (Figures 7C, S7B, S7C, and S7). The molecular chaperone HEAT SHOCK PROTEIN 90 (HSP90) delivers precursor proteins into chloroplasts.[42] BiFC

assay showed that CND1 interacts with HSP90 (Figure S7D), and the levels of HSP90 associated with CND1 consistently increased during 4-, 24-, and 48-h light treatments (Figures 7D and S7E), although *HSP90* transcripts reached their highest levels after 4 h of light induction but later declined (Figure S7D). These results suggest that light promotes CND1 import into chloroplasts via the molecular chaperone HSP90.

DISCUSSION

The proper functioning of cells depends on preserving the integrity of the cellular genome. In plant cells, very few genes are encoded by the chloroplast genome. Although the mechanisms underlying nuclear genome maintenance are well understood, little is known about the mechanisms that ensure genome stability of the semiautonomous organelles chloroplast and mitochondrion, and much less is known about the coordination of genome stability between the nucleus and chloroplasts. We identified a nucleus-encoded protein, CND1, that localized in the nucleus and chloroplasts and demonstrated that CND1 played dual roles in the maintenance of genome stability in both cellular compartments (Figure 7E).

Dual-localized proteins play important roles in coordinating functions across different subcellular components, although their identification has been limited.[43,44] Full-length CND1 was transported into the nucleus, but it was also targeted to chloroplasts, where its cTP was cleaved upon import and led to the accumulation of a truncated (mature) form of CND1 (Figure 1C). The predicted cTP and NLS sequences identified in CND1 control its distinct nuclear and chloroplast compartmentalization, respectively (Figure 1B). These localization characteristics are reminiscent of the chloroplast and nucleus dual-localized protein LEFKOTHEA (LEFKO), which plays dual roles in the regulation of chloroplast and nuclear mRNA splicing.[45] In contrast to LEFKO, CND1 does not contain a nuclear export signal. Several dual-localized proteins have distinct functions in different subcellular components. For instance, CDT1 localizes to chloroplasts and the nucleus. Nuclear CDT1 functions in gametophyte development and maintenance of genome integrity as a component of the DNA pre-replication initiation complex.[7] Chloroplast-localized CDT1 interacts with the chloroplast division factor ACCUMULATION AND REPLICATION OF CHLOROPLASTS 6 (ARC6) and likely participates in chloroplast division.[46] The complete loss of functions of CND1 (Figures 1B and 1C), LEFKOTHEA,[45] or CDT1[7] all lead to embryo lethality, suggesting their critical role in plant survival.

CND1 is required for the maintenance of nuclear genome stability. We showed that lower CND1 function increased endoreplication and genome instability (Figures 4A–4C), which is similar to the role of chloroplast and nuclear dual-localized CDT1 in the nucleus.[7] Nuclear genome instability may result from failure at different steps during the cell cycle, from DNA replication to chromosome segregation. Disruption of initiation of DNA replication is the most common cause of genome instability.[47] CND1 associated with DNA replication origins and members of the DNA pre-RC, which function during the early stages of DNA replication initiation (Figures 3A–3E). Loading of the MCM replicative helicase at origins of replication is required for initiation of DNA replication in all eukaryotes.[48,49] We established that CND1 directly interacted with the pre-RC protein MCM4 (Figures 3A and 3B) to promote the association of the pre-RC with origins of DNA replication (Figure S3F). This observation suggested that CND1 was involved in the maintenance of genome integrity by regulating the initiation of DNA replication in the nucleus. There is a strong relationship between DNA replication and transcription in plants.[31] CND1 is also associated with cell cycle- and DNA stability-related genes (Figure S3G) and altered their expression (Figure S4A; Table S5), suggesting another mechanism by which CND1 regulates genome stability and the cell cycle. MCM-Binding Protein (MCM-BP) is required for DNA replication and transcription in the protozoan parasite *Trypanosoma brucei*,[50] which has a role similar to that of CND1 in the regulation of DNA replication initiation in Arabidopsis. We identified differential peaks of DNA methylation between *cnd1-3* and wild-type plants that involved origins of DNA replication and cell cycle- and DNA stability-related genes (Figures S4B and S4C; Table S5), suggesting that DNA methylation probably plays a role in the nuclear genome stability.

Although CND1 has dual roles in chloroplast and nuclear genome stability, the underlying regulatory mechanism is unlikely to be identical. In chloroplasts, illegitimate recombination and DNA content increased in *cnd1-3* and *CND1*-RNAi lines (Figures 5A and 5B), suggesting that CND1 is also required for the maintenance of chloroplast genome stability. Furthermore, CND1 interacted with the chloroplast genome stability regulator WHY1 and facilitated its association with chloroplast DNA (Figures 5E, 5F, and 5G). Thus, CND1 mediates the association of the pre-RC with DNA in the nucleus and with DNA stability regulators in the chloroplast. Light drives photosynthesis, which generates ROS and increases chloroplast DNA damage.[51] Thus, maintenance of chloroplast DNA stability is crucial. We showed that light promotes *CND1* expression and CND1 transport to the chloroplast, the latter being mediated by HSP90, to maintain chloroplast genome stability. In the nucleus, the ZF motif of CND1 was necessary for its interaction with MCM4 (Figures 3A and 3B). All members of the MCM complex contain a ZF motif, which is vital for MCM complex formation and association with DNA,[5] similar to CND1. However, as the maturation of chloroplast-localized CND1 may remove parts of the ZF motif, how CND1 interacts with WHY1 is unclear.

The subpools of nuclear and chloroplast CND1 play distinct physiological roles in plants. The *cnd1-3* mutant and *CND1*-RNAi plants exhibited increased NPQ (Figures 5C and 5D), suggesting that the loss of CND1 function affects light harvesting capacity. However, partial loss of CND1 function in *cnd1-3* and the RNAi lines did not change maximum photochemical quenching (F_v/F_m), suggesting that the effect of CND1 on photosynthetic capacity is mild, with two potential caveats with this interpretation. First, the *cnd1-3* allele and *CND1*-RNAi do not completely abrogate *CND1* expression, since these genotypes are fully viable. Second, the partial loss of CND1 function may be compensated by redundant regulators of chloroplast genome stability. Similarly, *why1*, *why3*, *polIB*, or *RecA* single mutants do not have obvious chloroplast genome instability or overall altered growth phenotypes. Only the triple mutants *why1 why3*

polIB and *why1 why3 RecA* exhibit clear chloroplast genome instability and impaired growth.[13] Chloroplast-restricted CND1 functionally rescued the abnormal chlorophyll fluorescence seen in *cnd1-3*, indicating that the function of CND1 in chloroplasts contributes to the chlorophyll fluorescence phenotype (Figure 6B). Severe defects in DNA replication can result in embryo lethality. In addition, the disruption of DNA ploidy and the cell cycle have been reported to result in serrated leaves.[52,53] Accordingly, the leaves of *CND1* knockdown mutants and *CND1*-RNAi plants were distinctly serrated (Figure 2D). Nucleus-restricted CND1 functionally rescued the serrated leaves of the *cnd1-3* mutant (Figure 6B), suggesting that the function of CND1 in the nucleus contributes to leaf morphology.

The endosymbiosis theory states that organelles such as mitochondria and chloroplasts originated from endosymbiotic prokaryotes.[1] To coordinate their transcription, translation, and protein import with the host cell, organelles have evolved multiple strategies, including gene transfer to the nucleus,[1] and chloroplast-to-nucleus retrograde signaling.[54] The emergence of proteins with dual or multiple localization in eukaryotes may be a key strategy to coordinate molecular events between different organelles.[43] However, it is often difficult to identify dual-localized proteins due to their dynamic distribution in cells. For example, CND1 localized to the chloroplast and the nucleus in meristems (such as the shoot apex). However, CND1 mainly localized to the chloroplast in photosynthetic organs (such as leaves), but mainly localized to the nucleus in reproductive organs (such as seeds). Similarly, an LEFKO-yellow fluorescent protein (YFP) fusion showed a dual localization in the nucleus and protoplasts of embryonic cells. LEFKO-YFP is detected in the nuclei of lateral root meristem cells and localizes to both nuclei and chloroplasts in primary root meristems and leaf epidermal cells.[45] Immunoblot analysis of LEFKO-YFP verified that LEFKO is indeed targeted *in vivo* to both nuclei and chloroplasts, and that its dual localization is not due to the nuclear accumulation of free YFP arising from cleavage of the fusion protein,[45] which may be a concern in other cases. Some chloroplast proteins also localize to the nucleus, such as PLASTID TRANSCRIPTIONALLY ACTIVE (pTAC) proteins.[55–57] There may be many more dual- or multiple-localized proteins, and those currently identified may only comprise the tip of the iceberg.

Limitations of the study

Although our results have shown that dual-localized protein CND1 functions in the stability of nuclear and chloroplast genomes, we acknowledge that more investigations need to be performed to understand the underlying mechanisms.

The exact mechanism of how CND1 associates with MCM4 in the nucleus and WHY1 in chloroplasts to regulate the origin of DNA replication and plastid genome stability remains unclear. The resolution of the structure of CND1 could help clarify the exact molecular function of CND1 in the future. In addition, DNA methylation is affected in *cnd1-3*, the relationship between the alteration of DNA methylation and DNA replication origin remains to be clarified.

Last, the mechanism of how plants coordinate the localization of CND1 proteins to the nucleus and chloroplast remains unclear. Although the dual localization of CND1 in protoplast cells with two nuclei and the dual-localized distribution of CND1 protein in the shoot apex suggest that the genome states of plastid and nucleus are more needed to coordinate when the cells are in the stage of division, there is no direct evidence to show the cell with dual localization of CND1 is really dividing. Further studies are required for elucidating the coordination of localization and function of CND1 proteins in different tissues, which will provide insight to understand the mechanism of coordination between different organelles.

STAR★METHODS

Detailed methods are provided in the online version of this paper and include the following:

- KEY RESOURCES TABLE
- RESOURCE AVAILABILITY
  - Lead contact
  - Materials availability
  - Data and code availability
- EXPERIMENTAL MODEL AND SUBJECT DETAILS
  - Plant materials and growth conditions
- METHOD DETAILS
  - Light and fluorescence microscopy
  - Isolation of thylakoid membranes
  - Production of Anti-CND1 polyclonal antibodies
  - Reverse transcription quantitative PCR (RT-qPCR)
  - Chlorophyll fluorescence
  - Blue native-polyacrylamide gel electrophoresis (BN-PAGE) and immunoblot analyses
  - Flow cytometry
  - Yeast two-hybrid (Y2H) experiments
  - Detection of rearranged DNA by PCR
  - Immunoprecipitation
  - Analysis of *CND1* expression in different tissues
  - Methylated DNA immunoprecipitation sequencing (MeDIP-seq)
  - Chromatin immunoprecipitation (ChIP) and sequencing
  - Scanning electron microscopy
  - Differential interference contrast light microscopy
  - *In situ* detection of ROS
  - RNA sequencing
- QUANTIFICATION AND STATISTICAL ANALYSIS

SUPPLEMENTAL INFORMATION

Supplemental information can be found online at https://doi.org/10.1016/j.celrep.2023.112268.

ACKNOWLEDGMENTS

We thank ABRC for providing plant materials. We thank Professor Lizhen Tao (South China Agricultural University) for providing the DIC microscope for analysis. This work was supported by the National Natural Science Foundation of China Grant (Grant nos. 31970261, U22A20446, 32100192); and the Talent Support Project of Guangdong (2019TQ05N182).

AUTHOR CONTRIBUTIONS

H.-L.J. and H.-B.W. conceived the project. H.-L.J., S.D., P.Z., Y.Z., M.L., L.L., Z. Chen, and L.H. performed the experiments. H.-L.J., S.D., and H.-B.W. wrote the manuscript. Z.Y., Z.Chang, and J.H. revised the manuscript.

DECLARATION OF INTERESTS

The authors declare no competing interests.

Received: December 23, 2021
Revised: December 19, 2022
Accepted: February 28, 2023
Published: March 17, 2023

REFERENCES

1. Timmis, J.N., Ayliffe, M.A., Huang, C.Y., and Martin, W. (2004). Endosymbiotic gene transfer: organelle genomes forge eukaryotic chromosomes. Nat. Rev. Genet. *5*, 123–135.
2. Pfalz, J., and Pfannschmidt, T. (2013). Essential nucleoid proteins in early chloroplast development. Trends Plant Sci. *18*, 186–194.
3. Gould, S.B., Waller, R.F., and McFadden, G.I. (2008). Plastid evolution. Annu. Rev. Plant Biol. *59*, 491–517.
4. Masai, H., Matsumoto, S., You, Z., Yoshizawa-Sugata, N., and Oda, M. (2010). Eukaryotic chromosome DNA replication: where, when, and how? Annu. Rev. Biochem. *79*, 89–130.
5. Tuteja, N., Tran, N.Q., Dang, H.Q., and Tuteja, R. (2011). Plant MCM proteins: role in DNA replication and beyond. Plant Mol. Biol. *77*, 537–545.
6. Tye, B.K. (1999). MCM proteins in DNA replication. Annu. Rev. Biochem. *68*, 649–686.
7. Domenichini, S., Benhamed, M., De Jaeger, G., Van De Slijke, E., Blanchet, S., Bourge, M., De Veylder, L., Bergounioux, C., and Raynaud, C. (2012). Evidence for a role of Arabidopsis CDT1 proteins in gametophyte development and maintenance of genome integrity. Plant Cell *24*, 2779–2791.
8. Maréchal, A., Parent, J.S., Véronneau-Lafortune, F., Joyeux, A., Lang, B.F., and Brisson, N. (2009). Whirly proteins maintain plastid genome stability in Arabidopsis. Proc. Natl. Acad. Sci. USA *106*, 14693–14698.
9. Cappadocia, L., Maréchal, A., Parent, J.S., Lepage, E., Sygusch, J., and Brisson, N. (2010). Crystal structures of DNA-whirly complexes and their role in arabidopsis organelle genome repair. Plant Cell *22*, 1849–1867.
10. Krause, K., Kilbienski, I., Mulisch, M., Rödiger, A., Schäfer, A., and Krupinska, K. (2005). DNA-binding proteins of the Whirly family in Arabidopsis thaliana are targeted to the organelles. FEBS Lett. *579*, 3707–3712.
11. Shedge, V., Arrieta-Montiel, M., Christensen, A.C., and Mackenzie, S.A. (2007). Plant mitochondrial recombination surveillance requires unusual RecA and MutS homologs. Plant Cell *19*, 1251–1264.
12. Parent, J.S., Lepage, E., and Brisson, N. (2011). Divergent roles for the two PolI-like organelle DNA polymerases of Arabidopsis. Plant Physiol. *156*, 254–262.
13. Zampini, É., Lepage, É., Tremblay-Belzile, S., Truche, S., and Brisson, N. (2015). Organelle DNA rearrangement mapping reveals U-turn-like inversions as a major source of genomic instability in Arabidopsis and humans. Genome Res. *25*, 645–654.
14. Chan, K.X., Phua, S.Y., Crisp, P., McQuinn, R., and Pogson, B.J. (2016). Learning the languages of the chloroplast: retrograde signaling and beyond. Annu. Rev. Plant Biol. *67*, 25–53.
15. Calderon, R.H., and Strand, Å. (2021). How retrograde signaling is intertwined with the evolution of photosynthetic eukaryotes. Curr. Opin. Plant Biol. *63*, 102093.
16. Hernández-Verdeja, T., and Strand, Å. (2018). Retrograde signals navigate the path to chloroplast development. Plant Physiol. *176*, 967–976.
17. Mielecki, J., Gawroński, P., and Karpiński, S. (2020). Retrograde signaling: understanding the communication between organelles. Int. J. Mol. Sci. *21*, 6173.
18. Gray, J.C., Sullivan, J.A., Wang, J.H., Jerome, C.A., and MacLean, D. (2003). Coordination of plastid and nuclear gene expression. Philos. Trans. R. Soc. Lond. B Biol. Sci. *358*, 135–144. discussion: 144-145.
19. Shikanai, T., and Fujii, S. (2013). Function of PPR proteins in plastid gene expression. RNA Biol. *10*, 1446–1456.
20. Marín-Navarro, J., Manuell, A.L., Wu, J., and Mayfield, S.P. (2007). Chloroplast translation regulation. Photosynth. Res. *94*, 359–374.
21. Mayfield, S.P., Yohn, C.B., Cohen, A., and Danon, A. (1995). Regulation of chloroplast gene-expression. Annu. Rev. Plant Physiol. Plant Mol. Biol. *46*, 147–166.
22. Stern, D.B., Goldschmidt-Clermont, M., and Hanson, M.R. (2010). Chloroplast RNA metabolism. Annu. Rev. Plant Biol. *61*, 125–155.
23. Chi, W., Sun, X., and Zhang, L. (2013). Intracellular signaling from plastid to nucleus. Annu. Rev. Plant Biol. *64*, 559–582.
24. Petrillo, E., Godoy Herz, M.A., Fuchs, A., Reifer, D., Fuller, J., Yanovsky, M.J., Simpson, C., Brown, J.W.S., Barta, A., Kalyna, M., and Kornblihtt, A.R. (2014). A chloroplast retrograde signal regulates nuclear alternative splicing. Science *344*, 427–430.
25. Hudik, E., Yoshioka, Y., Domenichini, S., Bourge, M., Soubigout-Taconnat, L., Mazubert, C., Yi, D., Bujaldon, S., Hayashi, H., De Veylder, L., et al. (2014). Chloroplast dysfunction causes multiple defects in cell cycle progression in the Arabidopsis crumpled leaf mutant. Plant Physiol. *166*, 152–167.
26. Duan, S., Hu, L., Dong, B., Jin, H.L., and Wang, H.B. (2020). Signaling from plastid genome stability modulates endoreplication and cell cycle during plant development. Cell Rep. *32*, 108019.
27. Emanuelsson, O., Nielsen, H., Brunak, S., and von Heijne, G. (2000). Predicting subcellular localization of proteins based on their N-terminal amino acid sequence. J. Mol. Biol. *300*, 1005–1016.
28. Hua, S., and Sun, Z. (2001). Support vector machine approach for protein subcellular localization prediction. Bioinformatics *17*, 721–728.
29. Costas, C., de la Paz Sanchez, M., Stroud, H., Yu, Y., Oliveros, J.C., Feng, S., Benguria, A., López-Vidriero, I., Zhang, X., Solano, R., et al. (2011). Genome-wide mapping of Arabidopsis thaliana origins of DNA replication and their associated epigenetic marks. Nat. Struct. Mol. Biol. *18*, 395–400.
30. Vergara, Z., Sequeira-Mendes, J., Morata, J., Peiró, R., Hénaff, E., Costas, C., Casacuberta, J.M., and Gutierrez, C. (2017). Retrotransposons are specified as DNA replication origins in the gene-poor regions of Arabidopsis heterochromatin. Nucleic Acids Res. *45*, 8358–8368.
31. Sequeira-Mendes, J., Vergara, Z., Peiró, R., Morata, J., Aragüez, I., Costas, C., Mendez-Giraldez, R., Casacuberta, J.M., Bastolla, U., and Gutierrez, C. (2019). Differences in firing efficiency, chromatin, and transcription underlie the developmental plasticity of the Arabidopsis DNA replication origins. Genome Res. *29*, 784–797.
32. Sterken, R., Kiekens, R., Boruc, J., Zhang, F., Vercauteren, A., Vercauteren, I., De Smet, L., Dhondt, S., Inzé, D., De Veylder, L., et al. (2012). Combined linkage and association mapping reveals CYCD5;1 as a quantitative trait gene for endoreduplication in Arabidopsis. Proc. Natl. Acad. Sci. USA *109*, 4678–4683.
33. Ni, D.A., Sozzani, R., Blanchet, S., Domenichini, S., Reuzeau, C., Cella, R., Bergounioux, C., and Raynaud, C. (2009). The Arabidopsis MCM2 gene is essential to embryo development and its over-expression alters root meristem function. New Phytol. *184*, 311–322.
34. Kovalchuk, I., and Kovalchuk, O. (2016). Genome Stability From Virus to Human Application (Elsevier Press), pp. 409–424.
35. He, L., Zhao, C., Zhang, Q., Zinta, G., Wang, D., Lozano-Durán, R., and Zhu, J.K. (2021). Pathway conversion enables a double-lock mechanism to maintain DNA methylation and genome stability. Proc. Natl. Acad. Sci. USA *118*, e2107320118.

36. Jin, H., Liu, B., Luo, L., Feng, D., Wang, P., Liu, J., Da, Q., He, Y., Qi, K., Wang, J., and Wang, H.B. (2014). Hypersensitive to high light1 interacts with low quantum yield of photosystem II1 and functions in protection of photosystem II from photodamage in arabidopsis. Plant Cell *26*, 1213–1229.

37. Holt, N.E., Zigmantas, D., Valkunas, L., Li, X.P., Niyogi, K.K., and Fleming, G.R. (2005). Carotenoid cation formation and the regulation of photosynthetic light harvesting. Science *307*, 433–436.

38. Lepage, É., Zampini, É., and Brisson, N. (2013). Plastid genome instability leads to reactive oxygen species production and plastid-to-nucleus retrograde signaling in arabidopsis. Plant Physiol. *163*, 867–881.

39. Ferreira, P.C., Hemerly, A.S., Engler, J.D., van Montagu, M., Engler, G., and Inzé, D. (1994). Developmental expression of the arabidopsis cyclin gene cyc1At. Plant Cell *6*, 1763–1774.

40. Galbraith, D.W., Harkins, K.R., and Knapp, S. (1991). Systemic endopolyploidy in Arabidopsis thaliana. Plant Physiol. *96*, 985–989.

41. Barow, M. (2006). Endopolyploidy in seed plants. Bioessays *28*, 271–281.

42. Qbadou, S., Becker, T., Mirus, O., Tews, I., Soll, J., and Schleiff, E. (2006). The molecular chaperone Hsp90 delivers precursor proteins to the chloroplast import receptor Toc64. EMBO J. *25*, 1836–1847.

43. Krause, K., and Krupinska, K. (2009). Nuclear regulators with a second home in organelles. Trends Plant Sci. *14*, 194–199.

44. Krause, K., Oetke, S., and Krupinska, K. (2012). Dual targeting and retrograde translocation: regulators of plant nuclear gene expression can be sequestered by plastids. Int. J. Mol. Sci. *13*, 11085–11101.

45. Daras, G., Rigas, S., Alatzas, A., Samiotaki, M., Chatzopoulos, D., Tsitsekian, D., Papadaki, V., Templalexis, D., Banilas, G., Athanasiadou, A.M., et al. (2019). LEFKOTHEA regulates nuclear and chloroplast mRNA splicing in plants. Dev. Cell *50*, 767–779.e7.

46. Raynaud, C., Perennes, C., Reuzeau, C., Catrice, O., Brown, S., and Bergounioux, C. (2005). Cell and plastid division are coordinated through the prereplication factor AtCDT1. Proc. Natl. Acad. Sci. USA *102*, 8216–8221.

47. Aguilera, A., and García-Muse, T. (2013). Causes of genome instability. Annu. Rev. Genet. *47*, 1–32.

48. Dukaj, L., and Rhind, N. (2021). The capacity of origins to load MCM establishes replication timing patterns. PLoS Genet. *17*, e1009467.

49. Sánchez, H., McCluskey, K., van Laar, T., van Veen, E., Asscher, F.M., Solano, B., Diffley, J.F.X., and Dekker, N.H. (2021). DNA replication origins retain mobile licensing proteins. Nat. Commun. *12*, 1908.

50. Kim, H.S. (2019). Genome-wide function of MCM-BP in Trypanosoma brucei DNA replication and transcription. Nucleic Acids Res. *47*, 634–647.

51. Oldenburg, D.J., and Bendich, A.J. (2015). DNA maintenance in plastids and mitochondria of plants. Front. Plant Sci. *6*, 883.

52. De Veylder, L., Beeckman, T., Beemster, G.T., Krols, L., Terras, F., Landrieu, I., van der Schueren, E., Maes, S., Naudts, M., and Inzé, D. (2001). Functional analysis of cyclin-dependent kinase inhibitors of Arabidopsis. Plant Cell *13*, 1653–1668.

53. Wang, H., Zhou, Y., Gilmer, S., Whitwill, S., and Fowke, L.C. (2000). Expression of the plant cyclin-dependent kinase inhibitor ICK1 affects cell division, plant growth and morphology. Plant J. *24*, 613–623.

54. Nott, A., Jung, H.S., Koussevitzky, S., and Chory, J. (2006). Plastid-to-nucleus retrograde signaling. Annu. Rev. Plant Biol. *57*, 739–759.

55. Chen, M., Galvão, R.M., Li, M., Burger, B., Bugea, J., Bolado, J., and Chory, J. (2010). Arabidopsis HEMERA/pTAC12 initiates photomorphogenesis by phytochromes. Cell *141*, 1230–1240.

56. Liebers, M., Gillet, F.X., Israel, A., Pounot, K., Chambon, L., Chieb, M., Chevalier, F., Ruedas, R., Favier, A., Gans, P., et al. (2020). Nucleo-plastidic PAP8/pTAC6 couples chloroplast formation with photomorphogenesis. EMBO J. *39*, e104941.

57. Yoo, C.Y., Pasoreck, E.K., Wang, H., Cao, J., Blaha, G.M., Weigel, D., and Chen, M. (2019). Phytochrome activates the plastid-encoded RNA polymerase for chloroplast biogenesis via nucleus-to-plastid signaling. Nat. Commun. *10*, 2629.

58. Alexander, M.P. (1969). Differential staining of aborted and nonaborted pollen. Stain Technol. *44*, 117–122.

59. Zhang, Y., Su, J., Duan, S., Ao, Y., Dai, J., Liu, J., Wang, P., Li, Y., Liu, B., Feng, D., et al. (2011). A highly efficient rice green tissue protoplast system for transient gene expression and studying light/chloroplast-related processes. Plant Methods *7*, 30.

60. Robinson, H.H., and Yocum, C.F. (1980). Cyclicphotophosphorylation-reactionscatalyzed by ferredoxin, methyl viologen and anthraquinone sulfonate. Use of photochemical reactions to optimize redox poising. Biochim. Biophys. Acta *590*, 97–106.

61. Porra, R., Thompson, W., and Kriedemann, P. (1989). Determination of accurate extinction coefficients and simultaneous equations for assaying chlorophylls a and b extracted with four different solvents: verification of the concentration of chlorophyll standards by atomic absorption spectroscopy. Biochim. Biophys. Acta Bioenerget. *975*, 384–394.

62. Lu, Y., Hall, D.A., and Last, R.L. (2011). A small zinc finger thylakoid protein plays a role in maintenance of photosystem II in Arabidopsis thaliana. Plant Cell *23*, 1861–1875.

63. Schägger, H., Cramer, W.A., and von Jagow, G. (1994). Analysis of molecular masses and oligomeric states of protein complexes by blue native electrophoresis and isolation of membrane protein complexes by two-dimensional native electrophoresis. Anal. Biochem. *217*, 220–230.

64. Peng, L., Ma, J., Chi, W., Guo, J., Zhu, S., Lu, Q., Lu, C., and Zhang, L. (2006). Low PSII accumulation1 is involved in efficient assembly of photosystem II in Arabidopsis thaliana. Plant Cell *18*, 955–969.

65. Klostermann, E., Droste Gen Helling, I., Carde, J.P., and Schünemann, D. (2002). The thylakoid membrane protein ALB3 associates with the cpSecY-translocase in Arabidopsis thaliana. Biochem. J. *368* (*Pt 3*), 777–781.

66. Zhang, J., Liu, B., Li, M., Feng, D., Jin, H., Wang, P., Liu, J., Xiong, F., Wang, J., and Wang, H.B. (2015). The bHLH transcription factor bHLH104 interacts with IAA-leucine resistant3 and modulates iron homeostasis in Arabidopsis. Plant Cell *27*, 787–805.

67. Dong, Z., Xiao, Y., Govindarajulu, R., Feil, R., Siddoway, M.L., Nielsen, T., Lunn, J.E., Hawkins, J., Whipple, C., and Chuck, G. (2019). The regulatory landscape of a core maize domestication module controlling bud dormancy and growth repression. Nat. Commun. *10*, 3810.

68. Iberg-Badeaux, A., Collombet, S., Laurent, B., van Oevelen, C., Chin, K.-K., Thieffry, D., Graf, T., and Shi, Y. (2017). Transcription factor pulse can prime chromatin for heritable transcriptional memory. Mol. Cell Biol. *37*, e00372-16.

STAR★METHODS

KEY RESOURCES TABLE

REAGENT or RESOURCE	SOURCE	IDENTIFIER
Antibodies		
Mouse Anti-FLAG M2 affinity Gel	Sigma	Cat# A2220; RRID: AB_10063035
Rabbit Anti-CND1	This paper	N/A
Mouse Anti-GFP	TransGen Biotech	Cat# HT801-02; RRID:AB_2922385
Mouse Anti-FLAG M2, HRP Conjugate antibody	Sigma	Cat.#A8592; RRID: AB_439702
Rabbit Anti-D1	Agrisera	Cat# AS05084;RRID:AB_2172617
Rabbit Anti-D2	Agrisera	Cat# AS06146;RRID:AB_2172624
Rabbit Anti-CP43	Agrisera	Cat# AS06110; RRID:AB_1031781
Rabbit Anti-CP47	Agrisera	AS05920
Rabbit Anti-PsbO	Agrisera	Cat# AS05092;RRID:AB_1031788
Rabbit Anti-Cytf	Agrisera	Cat# AS08306;RRID:AB_2162096
Rabbit Anti-PsaA	Agrisera	Cat# AS06172;RRID:AB_2237771
Rabbit Anti-PsaD	Agrisera	Cat# AS09461;RRID:AB_1832088
Rabbit Anti-Lhca1	Agrisera	Cat# AS01005;RRID:AB_2135333
Rabbit Anti- Lhcb1	Agrisera	Cat# AS01004; RRID:AB_1832079
Rabbit Anti-ATPB	Agrisera	Cat# AS05085;RRID:AB_2063154
Rabbit Anti-HSP90	Agrisera	Cat# AS111629;RRID:AB_10772559
Rabbit Anti-H3	Agrisera	AS110710-100
Mouse Anti-MYC	TransGen Biotech	Cat# HT101;RRID:AB_2832251
Bacterial and virus strains		
Escherichia coli strain DH5a	TaKaRa	Cat# 9057
Agrobacterium tumefaciens strain EHA105	WEIDI	Cat#: AC1010
Chemicals, peptides, and recombinant proteins		
diaminobenzidine	newprobe	PB10214-1
Nitro blue tetrazolium	newprobe	PB10519-2
DCF	Invitrogen	Cat# C6827 RRID: 2049036
SOSG	Invitrogen	Cat# S36002
DAPI	Sigma	Cat# D8417
Critical commercial assays		
Prime Script RT Reagent Kit	TaKaRa	Cat# RR047A
SYBR Premix Ex Tag	TaKaRa	Cat# RR420A
CometAssay Kit	Trevigen	CAT# 4250-050-K
Deposited data		
ChIP-seq raw data for Arabidopsis: CND1-Flag, Col-0	https://www.ncbi.nlm.nih.gov/geo/	GSE220489
RNA-seq raw data for Arabidopsis: *cnd1-3*, Col-0	https://www.ncbi.nlm.nih.gov/geo/	GSE220490
MeDIP-seq raw data for Arabidopsis: *cnd1-3*, Col-0	https://submit.ncbi.nlm.nih.gov/subs/sra/	PRJNA907131
Experimental models: Organisms/strains		
Arabidopsis thaliana: Col-0 wild-type	This paper	N/A
Arabidopsis thaliana: *cnd1-1*/+	ABRC	SALK_152644
Arabidopsis thaliana: *cnd1-2*/+	ABRC	WiscDsLoxHs084_01H
Arabidopsis thaliana: *cnd1-3*	ABRC	SALK_058039C
Arabidopsis thaliana: *CND1*-RNAi22#	This paper	N/A
Arabidopsis thaliana: *CND1*-RNAi26#	This paper	N/A

(*Continued on next page*)

Continued

REAGENT or RESOURCE	SOURCE	IDENTIFIER
Arabidopsis thaliana:35S:CND1-Flag	This paper	N/A
Arabidopsis thaliana:35S:CND1 ^{NLS} -Flag	This paper	N/A
Arabidopsis thaliana:35S:CND1$^{\Delta cTP}$-Flag	This paper	N/A
Arabidopsis thaliana:35S:CND1$^{\Delta ZF}$-Flag	This paper	N/A
Oligonucleotides		
Primers for PCR and qPCR, see Table S7	This paper	N/A
Primers for mutant identification, see Table S7	This paper	N/A
Primers for ptDNA arrangement, see Table S7	This paper	N/A
Primers for ChIP-qPCR, see Table S7	This paper	N/A
Primers for vectors construction, see Table S7	This paper	N/A
Recombinant DNA		
35S:MCM4-Flag	This paper	N/A
35S:WHY1-Flag	This paper	N/A
pUC-CND1-GFP	This paper	N/A
pUC-CND1$^{\Delta cTP}$-GFP	This paper	N/A
pUC-CND1^{NLS}-GFP	This paper	N/A
pUC-MCM4-YN	This paper	N/A
pUC-MCM4^{ZF}-YN	This paper	N/A
pUC-CND1-YC	This paper	N/A
pUC-CND1$^{\Delta ZF}$-YC	This paper	N/A
pUC-WHY1-YN	This paper	N/A
pUC-WHY3-YN	This paper	N/A
pUC-PoliB-YN	This paper	N/A
pUC-RecA-YN	This paper	N/A
Software and algorithms		
Prism 6	GraphPad	N/A
ImageJ	NIH	N/A
CASP comet assay software	http://casplab.com/	http://casplab.com/
Other		
imaging-PAM	Walz	MAXI-Series
scanning electron microscopy	Hitachi	3400N
flow cytometry	Beckman	MoFlo XDP
laser scanning confocal microscope	Zeiss	Zen2011
differential interference microscope	OLYMPUS	BX51

RESOURCE AVAILABILITY

Lead contact

Further information and requests for resources and reagents should be directed to and will be fulfilled by the Lead Contact, Hong-Lei Jin (jinhl@gzucm.edu.cn).

Materials availability

All unique/stable reagents generated in this study are available from the lead contact with a completed Materials Transfer Agreement.

Data and code availability

Sequencing data are available at GEO in NCBI (https://www.ncbi.nlm.nih.gov/geo/) under accession numbers GEO: GSE220490 (RNA-seq); GEO: GSE220489 (ChIP-seq). Sequencing data are available at MeDIP-seq data are available at the Sequence Read Archive (SRA) at NCBI (https://submit.ncbi.nlm.nih.gov/subs/sra/) under accession number PRJNA907131.

This paper does not report original code. Any additional information required to reanalyze the data reported in this paper is available from the lead contact upon request.

EXPERIMENTAL MODEL AND SUBJECT DETAILS

Plant materials and growth conditions

All Arabidopsis (*Arabidopsis thaliana*) transfer DNA (T-DNA) insertion lines used in this study are in the Col-0 background. The *cnd1-1*, *cnd1-2* and *cnd1-3* mutants were obtained from the Arabidopsis Biological Resource Center (stock # SALK_152644, WiscDsLoxHs084_01H, and SALK_058039C, respectively). For observations of seeds, embryos and anthers, Arabidopsis plants were grown in soil in a long-day (16-h light/8-h dark, 21°C) growth chamber. For other experiments, Arabidopsis plants were grown in soil in a neutral-day (12-h light/12-h dark, 21°C) growth chamber.

Arabidopsis seeds were surface sterilized by treatment with Bayrochlor (Bayrol) for 20 min, followed by several washes in sterile water. Seeds were then hydrated in sterile water for 2 to 4 d at 4°C to induce homogeneous germination. Seeds were sown on half-strength Murashige and Skoog (MS) medium (Basalt Salt Mixture M0221; Duchefa) with appropriate antibiotics if needed and solidified with 0.8% (w/v) agar (Phyto-Agar HP696; Kalys) and grown in a long-day growth chamber at 21°C. After 2 weeks, seedlings were transferred to soil in a growth chamber in neutral-day conditions.

METHOD DETAILS

Light and fluorescence microscopy

Fresh siliques were opened under a stereomicroscope and images were captured with a charge-coupled device (CCD) camera (SteREO Lumar.V12, ZEISS). Developing embryos were observed by differential interference contrast microscopy, and images were obtained with a cooled CCD camera (OLYMPUS-BX51). Anthers were stained in Alexander solution to stain pollen grains and observed by light microscopy.[58]

Subcellular localization of GFP fusion proteins (Vec-GFP, control with empty vector; CND1-GFP, CND1-GFP fusion; CND1$^{\Delta cTP}$, CND1 lacking cTP; CND1$^{\Delta NLS}$, CND1 lacking NLS; AR4-mCherry) and bimolecular fluorescence complementation (BiFC) were performed as previously described.[59]

Isolation of thylakoid membranes

Thylakoid membranes were prepared as previously described.[60] The leaves were rapidly homogenized using mortar and pestle in 2–3 mL of grinding buffer (GB) containing 0.4 M sorbitol, 5 mM EDTA, 5 mM EGTA, 5 mM MgCl2, 10 mM $NaHCO_3$, 20 mM Tricine/NaOH (pH 8.4) and 0.5% (w/v) fatty acids-free BSA. The homogenate was filtered through 8 layers of cheesecloth, with a gentle hand pressure being applied in order to increase the final thylakoid yield. The suspension was centrifuged at 2,600 g for 3 min at 4°C, the supernatant carefully discarded and the pellet resuspended in 2–3 mL of resuspending buffer (RB) containing 0.3 M sorbitol, 2.5 mM EDTA, 5 mM $MgCl_2$, 10 mM $NaHCO_3$, 20 mM HEPES (pH 7.6) and 0.5% (w/v) fatty acids-free BSA. After centrifugation (2,600 g for 3 min at 4°C), the pellet was washed again in RB and then was resuspended in 1 mL of hypotonic buffer (HB) containing 2.5 mM EDTA, 5 mM MgCl2, 10 mM NaHCO3, 20 mM HEPES (pH 7.6) and 0.5% (w/v) fatty acids-free BSA, and the final volume was adjusted to 5 mL with HB. The thylakoid membranes were collected by centrifugation (2,600 g for 3 min at 4°C). Finally, the pellet was resuspended in a small volume (0.5–1 mL) of RB and the suspension was stored in ice in the dark until use. The chlorophyll concentrations from thylakoid preparations and from intact leaves were calculated from the absorbances at 645 and 663 nm of an 80% (v/v) acetone extract, Isolated thylakoid membranes were quantified based on total chlorophyll, as described.[61]

Production of Anti-CND1 polyclonal antibodies

Affinity-purified anti-CND1 polyclonal antibodies were produced by GenScript. A 15-amino-acid peptide (corresponding to amino acids 467–481 of Holoprosencephaly 1 [CND1]) with an additional N-terminal Cys residue, CFDKPEAKPARVEGK, was chemically synthesized, conjugated with keyhole limpet hemocyanin, and used to produce antibodies against CND1 in rabbits.

Reverse transcription quantitative PCR (RT-qPCR)

Total RNA was extracted from Arabidopsis rosette leaves with an RNeasy Plant Mini Kit (Qiagen). RNA samples were then reverse-transcribed into first-strand cDNAs with a PrimeScript RT Reagent Kit (TaKaRa). For RT-PCR, *UBIQUITIN 10* (*UBQ10*) was used as the control gene. Quantitative PCR was performed using gene-specific primers and SYBR Premix ExTaq reagent (TaKaRa) with a real-time RT-PCR System (RoChe-LC480), according to the manufacturer's instructions. Reactions were performed in triplicate for each sample, and expression levels were normalized against *ACTIN2* (*ACT2*) using the primers listed in Table S7.

Chlorophyll fluorescence

Chlorophyll fluorescence parameters were measured with the MAXI version of the IMAGING-PAM M-Series chlorophyll fluorescence system (Heinz-Walz Instruments). Plants were dark-adapted for 30 min before measurements were made, and light-response curves were determined as previously described.[62]

NPQ and light-response curves were determined as described.[36,62]

Blue native-polyacrylamide gel electrophoresis (BN-PAGE) and immunoblot analyses

BN-PAGE was performed as previously described[63] with modifications.[64] and loaded onto a 1 mm thick separation gel with a 5–13.5% acrylamide gradient. For two dimensional SDS-PAGE, excised BN-PAGE gel lanes were soaked in SDS sample buffer [100 mM Tris-HCl, pH 6.8, 2% SDS, 15% glycerol and 2.5% (v/v) b-mercaptoethanol] for 10 min at room temperature and layered onto 1.5 mm thick 15% SDS-polyacrylamide gels. The gels were stained with Coomassie brilliant blue G250. To quantify thylakoid proteins, gels were loaded on an equivalent chlorophyll basis in amounts ensuring that immunodetection was in the linear range. For immunoblot analysis, thylakoid proteins were solubilized and separated on 12% SDS–polyacrylamide gels. After electrophoresis, the protein were transferred to polyvinylidene difluoride (PVDF) membranes (Millipore) and probed using antibodies, Primary antibodies were produced in rabbits. Signals were detected with SuperSignal West Pico Chemiluminescent Substrate (Thermo Scientific). Antisera against photosynthetic proteins were purchased from Agrisera.

Flow cytometry

To isolate nuclei, tissues were chopped with a razor blade in 1 mL of Galbraith buffer (Galbraith, 1983) containing 1% (w/v) polyvinylpyrrolidone 10,000, 5 mM metabisulfite, and 5 mg/mL RNase I from a stock solution of 50 units/mg. The resulting supernatant was filtered onto two layers of Miracloth. Propidium iodide was added to the filtered supernatant to a final concentration of 50 μg/mL. The endoreplication levels of 5,000 to 10,000 stained nuclei were determined using a Cyflow SL flow cytometer (Partec) with a 532-nm solid state laser (100 mW) for excitation, with emission collected after a 590-nm long-pass filter.

Yeast two-hybrid (Y2H) experiments

Y2H constructs were obtained by LR recombination using Gateway technology. Gateway-compatible Y2H vectors were derived from the pGADT7 and pGBKT7 vectors and were a gift from Pascale Rossignol (John Innes Centre, Norwich, UK). CND1 or CND1$^{\Delta ZF}$-BD and MCM4-AD were co-transformed into yeast. CND1-BD/AD and MCM4-AD/BD were used as negative control. Yeast transformation and interaction assays were performed as described previously.[46]

Detection of rearranged DNA by PCR

PCR reactions were conducted using Ex Taq polymerase (Takara Bio Inc.) according to the manufacturer's instructions. The search for rearranged products was performed using a series of outward-facing oligonucleotides spaced by approximately 5–50 kb. A total of 19 PCR reactions was performed on each of two independent DNA samples from the wild type and all *CND1* mutant lines and analyzed by agarose gel electrophoresis. The DNA samples for all plants were pre-adjusted to the same amount of chloroplast genomic DNA using semi-quantitative amplification before performing outward-facing PCR. All visible DNA bands were isolated, cloned and sequenced.

Immunoprecipitation

Immunoprecipitation was performed as previously described[65] with minor modifications. For CND1 and HSP90, total proteins extracted from 1 g seedling different light treatments after 5 days of growth in the dark were solubilized in Co-IP buffer (10 mM HEPES (pH 7.5), 150 mM NaCl, 1 mM EDTA, 10% glycerol, 0.05% Triton X-100, 1 pierce protease inhibitor EDTA-free). For the other Co-IP experiments, total proteins from 1 g of 10-day-old seedlings were solubilized in Co-IP buffer. After centrifugation, the supernatant was preincubated with 40 μL Anti-FLAG M2 affinity Gel, Anti-GFP Nanobody Magarose Beads, or Anti-MYC Nanobody Magarose Beads at 4°C for 3 h. The resin was washed five times with ice-cold phosphate-buffered saline (PBS), and bound proteins were eluted with sodium dodecyl sulfate polyacrylamide gel electrophoresis (SDS-PAGE) sample buffer, resolved by SDS-PAGE, and subjected to immunoblot analysis.

Analysis of *CND1* expression in different tissues

The different tissues analyzed were as follows: cell culture, 4-d-old suspension cells; root, 2-week-old roots; seedling, 2-week-old whole seedlings; shoot apex, shoot apex extracted from all visible leaves and leaf primordia using a dissecting microscope; elongating leaf, leaves between 0.5 and 1 cm in length; mature leaf, fully expanded leaves with no signs of senescence; senescing leaf, mostly green with some yellowing; cauline leaf (1.5 cm), cauline leaves from the base of the inflorescence; flower, opened flowers; silique, fully formed but still green; seed, seeds were mature but not hard. The expression of CND1 and CYCB1; 1 across different tissues was detected using RT-qPCR.

Methylated DNA immunoprecipitation sequencing (MeDIP-seq)

Arabidopsis seedlings were quickly pulverized with a BioPulverizer (Bio Spec Products Inc.) on dry ice. Genomic DNA was extracted with Allprep DNA/RNA/Protein Mini Kit (Qiagen) according to the manufacturer's protocol. DNA was purified by phenol–chloroform extraction followed by ethanol precipitation.

DNA (1 μg) was spiked with 1 ng unmethylated lambda DNA (Promega), fragmented (average size 300 bp), end-repaired, A-tailed, and adapter-ligated using a Truseq DNA sample prep kit (Illumina) according to the manufacturer's protocol. Adapter-ligated DNA was gel-isolated (2% [w/v] agarose gel, DNA size ranging from 400 to 500 bp) and recovered using a QIAquick gel extraction kit (Qiagen). After clean-up with AMPure XP beads, bisulfite conversion was performed using an EpiTect Bisulfite kit (Qiagen) with

the following thermal cycles: 95°C for 5 min, 60°C for 25 min, 95°C for 5 min, 60°C for 85 min, 95°C for 5 min, 60°C for 175 min, 95°C for 5 min, 60°C for 180 min. After clean-up with AMPure XP beads, bisulfite-converted DNA was amplified with PfuTurbo Cx Hotstart DNA Polymerase with the following thermal cycles: 95°C for 5 min, 98°C for 30 s; 12 cycles of 98°C for 10 s, 65°C for 30 s, and 72°C for 30 s, followed by 72°C for 5 min. DNA was cleaned with AMpure XP beads, and stored at −30°C until use. Sequencing was performed on a HiSeq2000 using PE100 base format.

General quality control checks were performed with FastQC v0.8.0 (http://www.bioinformatics.babraham.ac.uk/projects/fastqc/). Each dataset was filtered for average base quality score (>20). Filtered datasets were aligned to the reference genome using Bismark v0.7.8 (parameters-X 10000 –non_bs_mm -n 2 -l 50 -e 70 –chunkmbs 1024), using Bowtie v0.12.842 as the underlying alignment tool. Mappings for all datasets generated from the same library were merged, and duplicates removed via the Bismark deduplication tool (deduplicate_bismark_alignment_output.pl). Mapped reads were then separated by genome and by source strand (plus or minus). The first four and last base of each read2 in all read pairs were clipped due to positional methylation bias, and any redundant mapped bases due to overlapping mates from the same read pair were trimmed to avoid bias in quantification of methylation status. Finally, the alignments for multiple libraries from the same plant were merged. Read pairs mapped to phage λ were used as a QC assessment to confirm that the observed bisulfite conversion rate was >99%. Read pairs mapped to the reference genome were used for downstream analysis.

Using the DSS R package v2.15.0, differentially methylated cytosines (DMCs) were identified by DSS with the callDML function (default parameters), and differentially methylated regions (DMRs) were identified with the callDMR function (all other parameters default). DMC and DMR calls were also made via Metilene v.0.2-6 (all other parameters default), with a p-value threshold of 0.05 and mean methylation difference of 0.2 for DMCs, and with a p-value threshold of 0.05 and mean methylation difference of 0.1 for DMRs. All DMR calls from both tools were subjected to additional filters, as described below. DMRs were required to contain at least 3 validated CpG sites and have a minimum length of 50 bp.

Chromatin immunoprecipitation (ChIP) and sequencing

ChIP was performed as described previously[66] with some modifications. 10 mL protoplasts (10^5 cells/mL) of *cnd1-3* or Col-0 transfected with *35S:WHY1-Flag* or *35S:MCM4-Flag* plasmid were used. After 18 h, transfected protoplasts were fixed in 1% (w/v) formaldehyde and then glycine was added to 0.125 M to titrate the remaining formaldehyde. The fixed tissue was washed 3 times with W5 solution. The protoplasts were harvested by centrifugation at 100 g for 3 min and resuspended in SDS lysis buffer (50 mM Tris-HCl at pH 7.5, 150 mM NaCl, 1 mM PMSF, 1 mM EDTA, 1% [w/v] SDS, 1% [v/v] Triton X-100, and 0.1% [w/v] sodiumdeoxycholate). Lysis was carried out on ice by sonicating thirty times for 10 s at power 3. The samples were kept on ice for 20 s between each interval. Then, 50 μL anti-FLAG M2 affinity gel (Sigma Aldrich) was used for each immunoprecipitation, Mouse Anti-FLAG M2 (Sigma Aldrich) were analyzed by immunoblotting, the amount of IP protein is related to the amount of total protein, and the enriched DNA fragments were analyzed by qPCR using the primers listed in Table S7 as previously described.[8,29]

The 25 μg amount of immunoprecipitated DNA was first normalized by comparing to the total input DNA used for each immunoprecipitation: $C_T = C_T\,(\text{ChIP}) - C_T\,(\text{input})$. Then, these normalized ChIP signals were compared to the input protein. The DNA binding of all plastid genes in Col-0 was set to 1, and these normalized ChIP signals in *cnd1-3* were compared to Col-0, and the related amount of DNA is showed in figure legends.

Immunoprecipitated DNA was used to construct sequencing libraries, following the protocol provided by the Illumina TruSeq ChIP Sample Prep Set A, and sequenced on an Illumina Xten instrument as 150-bp paired-end reads. Trimmomatic (version 0.38) was used to remove low-quality reads. Clean reads were mapped to the *Arabidopsis thaliana* genome by Bwa (version 0.7.15), allowing up to two mismatches. The potential PCR duplicates were removed by Samtools (version 1.3.1), and MACS2 software (version 2.1.1.20160309) was used to call peaks with default parameters (bandwidth,000 bp; model fold, 5, 50; q value, 0.05).[67] Wig files produced by MACS software were used for data visualization in IGV (version 2.3.91). The differential peaks was identified using Diffbind (version 1.16.3). The heatmaps and reads distribution of differential peaks and all peaks were obtained using Deeptool (version 3.2.1).[68]

Scanning electron microscopy

The second leaves of 28-d-old plants were fixed in 5% (w/v) glutaraldehyde, dehydrated in ethanol. CO_2 critical point drying was used to dry fixed leaves thoroughly. The epidermis surface was observed via scanning electron microscopy (Hitachi-3400N).

Differential interference contrast light microscopy

Fully formed but still green siliques of Col-0, *cnd1-1/CND1* and *cnd1-2/CND1* plants were decolorized in ethanol and then placed in clearing buffer (8 g chloral hydrate and 7.5 g Acacia Senegal dissolved in 60 mL of water and 5 mL of glycerol) for 1 h. The siliques were then peeled open and observed by light microscopy (Olympus CX31) using differential interference contrast microscopy, and images were obtained with a CCD camera.

In situ detection of ROS

In situ detection of ROS was performed using 3,3′-diaminobenzidine (DAB), nitroblue tetrazolium (NBT), and singlet oxygen sensor green (SOSG) reagent fluorometric probes (FluorChem Q Imaging System; excitation 504 nm and emission 525 nm) as previously

described.[36,62] Total ROS production was detected with a 2′,7′-dichlorofluorescin diacetate fluorometric probe (FluorChem Q Imaging System; excitation 488 nm and emission 525 nm). ROS fluorescence was analyzed by ImageJ.

RNA sequencing

Total RNA was extracted from *cnd1-3* and Col-0 seedlings using TRIzol Reagent according to the manufacturer's instructions (Magen). RNA quality was determined based on the A260/A280 absorbance ratio with a Nanodrop ND-2000 system (Thermo Scientific, USA), and the RIN (RNA integrity number) of RNA was determined on an Agilent Bioanalyzer 4150 system (Agilent Technologies, CA, USA). Only high-quality samples were used for library construction. Paired-end libraries were prepared using an ABclonal mRNA-seq Library Prep Kit (ABclonal, China) following the manufacturer's instructions. mRNA was purified from 1 μg total RNA using oligo (dT) magnetic beads followed by fragmentation carried out using divalent cations at elevated temperatures in ABclonal First Strand Synthesis Reaction Buffer. Subsequently, first-strand cDNAs were synthesized with random hexamer primers and reverse transcriptase (RNase H) using mRNA fragments as templates, followed by second-strand cDNA synthesis using DNA polymerase I, RNAse H, buffer, and dNTPs. The synthesized double-stranded cDNA fragments were then adapter-ligated for preparation of the paired-end library. Adapter-ligated cDNAs were used for PCR amplification. PCR products were purified (AMPure XP system) and library quality was assessed on an Agilent Bioanalyzer 4150 system. Finally, the libraries were sequenced on a MGISEQ-T7 instrument as 150-bp paired-end reads. The data generated from the BGI platform were used for bioinformatics analysis. All analyses were performed using an in-house pipeline from Shanghai Applied Protein Technology. Raw data (or raw reads) in fastq format were first processed through in-house perl scripts. In this step, the adapter sequences were removed and low quality reads (the number of lines with a string quality value below or equal to 25 accounted for more than 60% of the entire reading) were removed and N (N means that the base information cannot be determined) ratio greater than 5% reads to obtain clean reads for subsequent analysis. Then, clean reads were separately aligned to the reference genome in orientation mode using HISAT2 software (http://daehwankimlab.github.io/hisat2/) to obtain mapped reads. FeatureCounts (http://subread.sourceforge.net/) was used to count the read numbers mapping to each gene, then the FPKM of each gene was calculated based on the length of the gene and reads count mapped to this gene. Differential expression analysis was performed using the DESeq2 (http://bioconductor.org/packages/release/bioc/html/DESeq2.html) package. DEGs with $|\log2FC| > 1$ and $P\text{-adj} < 0.05$ were considered to be significantly differentially expressed genes. ClusterProfiler R software package was used for GO function enrichment and KEGG pathway enrichment analysis. A GO or KEGG function was considered significantly enriched at $p < 0.05$.

QUANTIFICATION AND STATISTICAL ANALYSIS

In this study, significant differences between two samples were determined with Two-tailed paired Student's t test. Error bars represent standard error of mean, 'n' represents the sample size, as mentioned in the figure legends. And asterisks indicate the statistical significance: *, $p < 0.05$; **, $p < 0.01$; ***, $p < 0.001$. At least three biological replicates were included. Statistical analysis was performed by GraphPad Prism 6. Leaf area, cell area, cell number were analysis by ImageJ. Comet assay was analysis by CASP comet assay software from http://casplab.com/.